RM L54I22

Copy 179
RM L54I22

NACA RM L54I22

NACA

RESEARCH MEMORANDUM

EXPERIMENTAL INVESTIGATION OF EFFECTS OF PRIMARY JET FLOW AND SECONDARY FLOW THROUGH A ZERO-LENGTH EJECTOR ON BASE AND BOATTAIL PRESSURES OF A BODY OF REVOLUTION AT FREE-STREAM MACH NUMBERS OF 1.62, 1.93, AND 2.41

By Robert M. O'Donnell and Russell W. McDearmon

Langley Aeronautical Laboratory
Langley Field, Va.

NATIONAL ADVISORY COMMITTEE
FOR AERONAUTICS

WASHINGTON
December 6, 1954

NATIONAL ADVISORY COMMITTEE FOR AERONAUTICS

RESEARCH MEMORANDUM

EXPERIMENTAL INVESTIGATION OF EFFECTS OF PRIMARY JET FLOW AND SECONDARY FLOW THROUGH A ZERO-LENGTH EJECTOR ON BASE AND BOATTAIL PRESSURES OF A BODY OF REVOLUTION AT FREE-STREAM MACH NUMBERS OF 1.62, 1.93, AND 2.41

By Robert M. O'Donnell and Russell W. McDearmon

SUMMARY

An investigation was made at free-stream Mach numbers of 1.62, 1.93, and 2.41 to determine the effects of a primary jet and secondary air flow on the base pressure and pressures acting over the boattail surface of a body of revolution for two secondary discharge areas. The Mach numbers of the primary nozzles were 1 and 3.23 with the secondary mass flow being varied from 0 to 10 percent of the primary mass flow. The ratio of jet stagnation temperature to tunnel stagnation temperature was about 0.96. The Reynolds number range of the investigation was from 2.1×10^6 to 2.9×10^6 based on body length. All testing was conducted with a turbulent boundary layer along the model.

This report presents results obtained with a zero-length ejector and covers jet static-pressure ratios from the jet-off condition to a maximum of about 128 for the sonic nozzle and to a maximum of about 9 for the supersonic nozzle.

INTRODUCTION

Many experiments (for example, refs. 1 to 6) have shown that a propulsive jet can affect the afterbody and base pressures considerably when it is being discharged through the base of a body of revolution. However, comparatively little is known about the magnitude of these effects when a secondary or cooling air flow is operated in conjunction

with the primary jet flow. The small amount of data presently available on the subject appears to be that from the investigations of references 3 and 4.

Because of this lack of experimental information and the inherent difficulties in a theoretical analysis, the present investigation of the effects of secondary air flow was undertaken. In view of the lack of experimental data for higher jet static-pressure ratios and of the fact that some present-day rocket-powered research aircraft operate at pressure ratios greater than 30 (future aircraft will probably operate at considerably higher ratios), the present investigation was made over a wide range of jet static-pressure ratios. The jet static-pressure ratio was varied from the jet-off value to a maximum of about 128 for the sonic nozzle and from the jet-off value to a maximum of about 9 for the supersonic nozzle.

This investigation is part of a general program to investigate various ejector lengths. For each ejector length the variables are free-stream Mach number, primary jet Mach number, secondary exit diameter, and secondary mass flow. The results presented herein were obtained from a zero-length ejector.

SYMBOLS

D diameter, in.

d secondary diameter of shroud, in.

H total pressure of secondary air flow, lb/sq in.

L total length of jet model, in.

M free-stream Mach number

P pressure coefficient, $\frac{p - p_s}{q}$

p static pressure, lb/sq in.

q free-stream dynamic pressure, lb/sq in.

w ratio of secondary mass flow to primary jet flow

x axial distance measured from model nose, in.

z axial distance measured from model base, in.

Subscripts:

B base of model

j primary jet

s free-stream condition

APPARATUS

Wind Tunnel

All tests were conducted in the Langley 9-inch supersonic tunnel, which is a continuous-operation, closed-circuit type in which the pressure, temperature, and humidity of the enclosed air can be regulated. Different test Mach numbers are provided by interchangeable nozzle blocks which form test sections approximately 9 inches square. Eleven fine-mesh turbulence-damping screens are installed ahead of the supersonic nozzle in a settling chamber of relatively large area. A schlieren optical system is provided for qualitative flow observations.

Model and Auxiliary Apparatus

A sketch of the model used in the present investigation is shown in figure 1. The model body was 8.25 inches long and was constructed entirely of stainless steel. It consisted of a 20° conical nose, a cylindrical center section, and two interchangeable afterbodies of identical profiles. As shown in figure 1, the afterbodies had circular-arc boattails with a slope at the base of approximately 22°. This high degree of boattailing was adopted to simulate generally the trend in boattailing of many existing and proposed aircraft. The model afterbodies or shrouds had, within machining accuracy, the same external ordinates and differed only in their secondary discharge areas. The exit Mach number of the primary jet was varied from sonic ($M = 1$) to supersonic ($M = 3.23$) by the insertion of the supersonic nozzle through the sonic nozzle and into the primary stagnation chamber. The edge of the supersonic nozzle was sealed with solder to prevent leakage. Since the supersonic nozzle was tapered to a sharp edge at the exit, both nozzles had essentially the same exit area. Air was supplied to the supersonic nozzle through slots that were located longitudinally along the cylindrical portion of the nozzle insert.

The model was mounted from the tunnel sidewalls by the use of two wing struts. High-pressure air was supplied to the primary stagnation chamber by means of one wing strut constructed entirely of tubing and

silver solder and faired to a circular-arc cross section. The air to the secondary was supplied through the other wing strut in the same way except that part of this wing was used as an instrumentation conduit. The total temperature of the air in the model stagnation chamber was about 80° F, whereas that of the tunnel was approximately 100° F.

Pressure distributions were measured over the boattail by means of static-pressure orifices that were located as shown in figure 1. Base-pressure orifices were located at 90° intervals around the annuli of both shrouds with two of the four orifices in line with the wing struts.

TESTS AND PROCEDURE

Tests were conducted at free-stream Mach numbers of 1.62, 1.93, and 2.41 with a stagnation pressure of approximately 1 atmosphere; the corresponding Reynolds number range was from 2.1×10^6 to 2.9×10^6 based on body length. The dewpoint of the tunnel was kept sufficiently low in order to insure negligible condensation effects.

All testing was done at 0° angle of attack and with a turbulent boundary layer along the model. The latter was accomplished by use of a 1/8-inch salt band placed approximately $1\frac{1}{4}$ inches from the model nose. (See fig. 1.)

The afterbody and base pressures were recorded for both shrouds for the jet-off condition and up to primary jet static-pressure ratios of about 128 for the sonic nozzle and about 9 for the supersonic nozzle. Examination of the data revealed that the support struts had no apparent effect on the base pressure and, hence, an average value obtained from the four orifices was used.

Primary total pressures, measured by means of a calibrated total-pressure tube placed in the stagnation chamber ahead of the nozzle, were recorded on a mercury manometer for values less than 50 lb/sq in. and on precision gages for higher values. Jet static pressures were calculated from the measured total pressures on the basis of the exit Mach number as determined from the measured area ratio. Primary mass flows for both nozzles were calculated by using the measured total pressure and assuming the nozzle to be choked at the minimum area. Secondary mass flows of 0 to 10 percent of the primary mass flow were measured directly by means of calibrated rotameters.

PRECISION

Model alinement was maintained within ±0.1° of zero pitch and yaw with respect to the tunnel center line. Based on past surveys of the stream, the free-stream Mach number is accurate to within ±0.01, whereas the base pressure coefficient is accurate to within approximately ±0.003.

Secondary mass-flow ratios are estimated to be within ±0.2 percent, whereas total recorded pressures in the jet model are accurate to within ±0.01 inch of mercury for pressures less than 50 lb/sq in. and ±0.50 inch of mercury for pressures greater than 50 lb/sq in.

RESULTS AND DISCUSSION

Experimental and theoretical boattail pressure distributions are first compared for the case of no jet flow. The rest of the discussion is then divided into two parts: the first part concerning the sonic nozzle, and the last the supersonic nozzle. Each part consists of the primary and secondary jet effects on pressures acting over the base and boattail.

No Jet

Experimental boattail pressure distributions for both shrouds are compared with those obtained by the method of characteristics (15-point calculation) in figure 2 for free-stream Mach numbers of 1.62, 1.93, and 2.41. With the exception of those points lying in the regions of separated flow, the agreement between experiment and theory is considered good.

The difference in pressure distribution between the shrouds is probably associated with small changes in separation caused by the slightly different external shroud contours and orifice installations. However, these construction differences are within the machining accuracy of duplicating the shrouds and are not expected to affect the final results.

Sonic Nozzle

Base pressure.- Figure 3 illustrates the effects of the secondary mass flow and jet static-pressure ratio on pressures acting over the annular base of the first shroud $(d/D_B = 0.82)$. Base pressure coefficients corresponding to no primary or secondary flow are denoted by small arrows on the ordinates.

For the lower jet static-pressure ratios, the effects of the primary jet alone on the base pressure are substantially the same as those observed in references 2 and 3 which cover jet static-pressure ratios up to about 9. Initially, there may be a base-pressure increase from the no-flow value, such as that measured at $M = 1.62$. Then a reduction in base pressure occurs until a minimum base pressure coefficient is reached at $p_j/p_s \approx 2$. There is then an increase in base pressure with jet static-pressure ratio, with the base pressure coefficient attaining positive values. This type of variation has been discussed in references 2, 3, 7, 8, and 9 where the mechanism, by which the primary jet alone varies the base pressure, has been explained in terms of base bleed at very low jet static-pressure ratios and by the concept of the critical pressure-rise coefficient for higher pressure ratios. A typical full-size schlieren photograph is first presented in figure 4 in order to clarify some details of the flow phenomena. Schlieren photographs of the sonic jet alone operating at different static-pressure ratios and a free-stream Mach number of 1.62 are given in figure 5. The increases in base pressure due to the secondary flow are apparently brought about by the inability of the primary jet to maintain its scavenging effect upon the base and at the same time transport the increasing mass of secondary air. No suitable explanation has been found for the decrease in base pressure with the addition of secondary flow that occurs for some pressure ratios at $M = 2.41$ or for the decrease observed with the primary alone at very high jet static-pressure ratios.

Figure 6 illustrates the effects of secondary mass flow of the second shroud $\left(d/D_B = 0.73\right)$ on the base pressure. It should be noted that the base pressures on the second shroud due to secondary flow are lower than those of the first shroud. However, secondary mass-flow effects are, in general, qualitatively the same for both shrouds at all free-stream Mach numbers. At all Mach numbers it appears logical to expect that, for a given secondary mass flow and jet static-pressure ratio, the base pressure for the smaller secondary annulus area (second shroud) would be less than that for the larger secondary annulus area (first shroud), since the exit velocity of the secondary flow is greater for the smaller secondary annulus area. For a given secondary annulus area and jet static-pressure ratio, increasing the secondary mass flow would also increase the exit velocity of the secondary flow; however, the experimental results indicate that this increase in velocity is apparently offset by the increased mass of secondary air introduced in the vicinity of the base and by the inability of the scavenging action of the jet and outer stream to transport this additional mass downstream. For a given jet static-pressure ratio but different secondary annulus areas, it is possible to have a secondary exit velocity for the larger secondary annulus area that is equal to the secondary exit velocity for the smaller secondary annulus. However, such conditions require a secondary mass

flow from the larger secondary annulus that is much greater than that for the smaller secondary annulus; consequently, the base pressure for the larger annulus area would be expected to be higher for the reasons previously given. For both shrouds and at all Mach numbers, the greater part of the effect of secondary mass flow on base pressure occurred when the mass flow was increased from no flow to 2 percent of the primary flow.

Although the primary-alone data are obtained from the first shroud, the lower base pressures on the second shroud at $M = 2.41$ could not be attributed to a difference in construction, because the base pressures show good agreement when the primary and secondary flows are not operating. Also, from unpublished data, it has been found that any small initial base-pressure difference is for the most part eliminated when the jet is operated. Again, no explanation could be found for the reductions caused by the secondary flow at $M = 2.41$.

Boattail pressure distribution.- The effect of the primary jet and the secondary mass flow on the boattail pressures of the first shroud $\left(d/D_B = 0.82\right)$ is shown in figure 7 for free-stream Mach numbers of 1.62, 1.93, and 2.41, respectively. A comparison of these figures with the no-jet-flow case of figure 2 shows that the effect of the primary jet alone at $M = 1.62$ and 1.93 is, in general, to decrease the rearward boattail pressures at the lower static-pressure ratios and then to increase these pressures as the jet static-pressure ratio is increased, with an accompanying forward movement of the separation point. The primary jet alone at $M = 2.41$ appeared to increase the rearward boattail pressures as the jet static-pressure ratio was increased. These variations in the boattail pressures are similar to the variation in base pressure discussed previously.

At free-stream Mach numbers of 1.62 and 1.93, the effects of the secondary flow when operating with the primary jet are to increase the rearward boattail pressures and, in general, to cause the separation point to move slightly further forward. Secondary mass-flow effects at $M = 2.41$ over the boattail are small and irregular at the lower pressure ratios. At the highest jet static-pressure ratio, a substantial increase in the rearward boattail pressures occurred.

Schlieren photographs of the flow obtained with increasing mass-flow ratios and when the rearward boattail pressures were increasing are presented in figure 8 for a free-stream Mach number of 1.62 and a jet static pressure ratio of 4.65. From the photographs it can be seen that the boundary layer separates over the rearward part of the boattail. Therefore, since the rearmost boattail orifices lie in a separated region that also includes the base, the base pressure and the rearward boattail pressures increase simultaneously.

The increased boattail pressure rise due to the secondary flow is probably a result of the higher pressure of the secondary air bleeding through the already separated region over the boattail and of the reduced induction effects of the primary jet on the boattail brought about by the inability of the primary jet to maintain these induction effects while transporting the increasing mass of secondary air.

Figure 9 shows the effects of the primary and secondary flow on the boattail pressure distributions of the second shroud $\left(d/D_B = 0.73\right)$. (It should be noted here that the primary-alone distributions are those of the first shroud since no primary-alone data were obtained for the second shroud.) As can be seen from figure 9(a), the effect of the secondary mass flow at $M = 1.62$ is to increase the rearward boattail pressures and in some cases to cause a slight movement of the separation point. The action of the secondary mass flow on the pressures nearest the base at $M = 1.93$ (fig. 9(b)) is to lower them at the lowest pressure ratio and then to increase them progressively as the pressure ratio is increased with an accompanying slight forward movement of the separation point. At $M = 2.41$ (fig. 9(c)), the secondary mass flow decreased the rearward boattail pressures at the lower jet pressure ratios and increased them above those obtained with the primary jet operating alone at the highest pressure ratio (104.4). Schlieren photographs illustrating the secondary-flow effects with the second shroud at a free-stream Mach number of 1.62 and a jet static-pressure ratio of 3.10 are given in figure 10.

Supersonic Nozzle

Base pressure.- The variation of base pressure coefficient on the first shroud with jet static-pressure ratio and secondary mass-flow ratio is shown in figure 11 for all free-stream Mach numbers. When compared with the sonic nozzle it was found that the supersonic nozzle aspirated the base annulus to a lower minimum pressure, very likely because of its higher jet-boundary velocity. After reaching a minimum value, the base pressure then followed the same trend as the sonic nozzle. The reason for the increase in base pressure due to the addition of the secondary mass flow has been discussed previously with regard to the sonic nozzle. Schlieren photographs illustrating the supersonic nozzle operating alone at a free-stream Mach number of 1.62 and at various pressure ratios are presented in figure 12.

Figure 13 presents base pressures measured on the second shroud with the primary jet flow and secondary mass flow. As in tests with the first shroud, the addition of secondary mass flow increased the base pressures substantially at all jet static-pressure ratios. However, the increases in base pressure on the second shroud due to secondary mass flow are less

than those of the first shroud. The reasons for this have been explained previously in the discussion of the results for the sonic nozzle.

Boattail pressure distribution.- Afterbody pressure distributions for the first shroud $(d/D_B = 0.82)$ are presented in figure 14 for free-stream Mach numbers of 1.62, 1.93, and 2.41, respectively. Comparison of the pressure distributions of figure 14 with those of figure 2 shows that the effect of the supersonic nozzle when operating alone is to decrease the rearward boattail pressures at almost all jet static-pressure ratios. Apparently, the high velocity of the jet boundary produces a large induction effect upon the flow over the rearward portion of the boattail, thereby reducing separation and decreasing the rearward boattail pressures.

The addition of secondary mass flow with its lower energy air reduces the induction effects of the primary jet and causes the rearward boattail pressures to increase. Some pressures obtained at the higher jet static-pressure ratios become, as might be expected, larger than those of the no-jet-flow case. Schlieren photographs are presented in figure 15 for a free-stream Mach number of 1.62 in order to illustrate the flow of the supersonic nozzle with various secondary mass-flow ratios. It is interesting to note that a propulsive jet exhausting from the base of a body of revolution may, in practical application, be separated from the supersonic external stream by a subsonic mixing zone. This is evidenced by the fact that the shocks that arise within the jet do not pass through the mixing zone into the outer stream and by the tendency of the jet to exhibit periodic structure.

Boattail pressure distributions for the second shroud $(d/D_B = 0.73)$ are presented in figure 16 at free-stream Mach numbers of 1.62, 1.93, and 2.41, respectively. Secondary mass-flow effects at a Mach number of 1.62 for this shroud are the same as those of the first in that the secondary mass flow increases the rearward boattail pressures over that of the jet alone. Secondary mass-flow effects are different, however, at the two higher Mach numbers of 1.93 and 2.41. At a Mach number of 1.93, the addition of a secondary mass flow from the second shroud caused pressures at the most rearward orifice to increase at all jet static-pressure ratios and caused some forward pressures to decrease and approach the theoretical jet-off pressures at the lower jet static-pressure ratios. At a Mach number of 2.41, the secondary flow increased the rearward pressures at the higher jet static-pressure ratios only and decreased some forward pressures at the lower jet static-pressure ratios. An inspection of schlieren photographs obtained at lower jet static-pressure ratios revealed the presence of a shock wave originating on the rearward part of the boattail. When the secondary mass flow was operated, there appeared to be a downstream movement of the shock wave accompanied by a reduction in the forward pressures and area of separation over the

boattail. Because of this reduction, some forward pressures more nearly approached that obtained by the method of characteristics. Schlieren photographs obtained at $M = 1.62$ for the supersonic nozzle operating at a pressure ratio of about 0.92 together with secondary mass flow are presented in figure 17. At the higher secondary mass-flow ratios the jet structure and pattern in the vicinity of the secondary annulus shows similarity to the patterns observed in reference 10 for adjacent jets exhausting supersonically. A rough estimation based upon measured total and static pressures of the secondary flow indicated that the secondary annulus may be choked at the higher secondary mass flows and operate as an annular sonic exit.

Secondary Mass Flow Only

Base pressure.- Figure 18 presents the effects of the secondary mass flow alone on the base pressure of both shrouds. These effects are similar to those of reference 7 in that the base pressure reaches a maximum when the secondary total-pressure ratio is near 1 and then decreases as the secondary pressure and mass flow is increased. It should be noted here that at the higher rates of mass flow the secondary annuli of the shrouds operated as an annular sonic nozzle. Schlieren photographs illustrating secondary alone flow conditions are given in figure 19 for the first shroud at a Mach number of 1.62.

Boattail pressure distribution.- Figure 20 shows the effects of secondary mass flow on the boattail pressure distributions of both shrouds. Because of the erratic behavior of these distributions it is difficult to draw any general conclusions as to the effects of secondary flow alone other than that they are more pronounced at $M = 1.62$.

CONCLUSIONS

An investigation has been made at free-stream Mach numbers of 1.62, 1.93, and 2.41 to determine the effects of primary and secondary air flow on the base pressure and pressures acting over the boattail surface of a body of revolution for two secondary discharge areas. From the results of the investigation the following conclusions are indicated:

Sonic Nozzle

1. For the lower jet static-pressure ratios, the effect of the primary jet alone on the base pressure was the same as that described in NACA RM E51F26 which covers jet static-pressure ratios up to about 9. At higher jet static-pressure ratios the trend at these lower pressure

ratios continued, but at very large jet static-pressure ratios the base pressure began to decrease.

2. The addition of a secondary mass flow caused the base pressure to increase for both secondary discharge areas at Mach numbers of 1.62 and 1.93 but decreased the base pressure in some instances at a Mach number of 2.41. At all Mach numbers the greater part of the effect of secondary mass flow on base pressure occurred when the mass flow was increased from no flow to 2 percent of the primary flow.

3. At free-stream Mach numbers of 1.62 and 1.93, the primary jet alone first decreased the rearward boattail pressures and then increased them as the jet static-pressure ratio was increased. However, at a free-stream Mach number of 2.41, the primary jet alone increased the rearward boattail pressures at all jet static-pressure ratios.

4. For the larger secondary discharge area, the rearward boattail pressures were increased at Mach numbers of 1.62 and 1.93 by the addition of the secondary mass flow. At a Mach number of 2.41, the effects on the boattail pressures due to secondary mass flow were small and irregular. For the smaller secondary discharge area, rearward boattail pressures were increased at a Mach number of 1.62 by the addition of the secondary mass flow. At free-stream Mach numbers of 1.93 and 2.41, however, the secondary flow first decreased the rearward pressures and then increased them as the primary jet static-pressure ratio was increased.

Supersonic Nozzle

1. The effect of the primary jet alone at the low jet pressure ratios is to decrease the base pressure to a lower minimum value than that of the sonic nozzle. After the minimum value is reached, the trend is the same as for the sonic nozzle as the jet pressure ratio is increased.

2. The addition of secondary mass flow caused the base pressures to increase for both secondary discharge areas at all Mach numbers, with the greatest increase being obtained with the larger secondary discharge area.

3. The primary jet alone caused the rearward boattail pressures to decrease at the lower primary jet static-pressure ratios.

4. For the larger secondary discharge area, the rearward boattail pressures were generally increased at all Mach numbers by the addition of secondary mass flow. For the smaller secondary discharge area, the addition of secondary mass flow caused the rearward boattail pressures

to increase at all jet static-pressure ratios at Mach numbers of 1.62 and 1.93 only. At Mach numbers of 1.93 and 2.41, some forward pressures were decreased at the lower jet static-pressure ratios.

Langley Aeronautical Laboratory,
National Advisory Committee for Aeronautics,
Langley Field, Va., September 14, 1954.

REFERENCES

1. Love, Eugene S.: Aerodynamic Investigation of a Parabolic Body of Revolution at Mach Number of 1.92 and Some Effects of an Annular Jet Exhausting From the Base. NACA RM L9K09, 1950.

2. Cortright, Edgar M., Jr., and Schroeder, Albert H.: Investigation at Mach Number 1.91 of Side and Base Pressure Distributions Over Conical Boattails Without and With Jet Flow Issuing From Base. NACA RM E51F26, 1951.

3. Cortright, Edgar M., Jr., and Kochendorfer, Fred D.: Jet Effects on Flow Over Afterbodies in Supersonic Stream. NACA RM E53H25, 1953.

4. Gorton, Gerald C.: Pumping and Drag Characteristics of an Aircraft Ejector at Subsonic and Supersonic Speeds. NACA RM E54D06, 1954.

5. Englert, Gerald W., Vargo, Donald J., and Cubbison, Robert W.: Effect of Jet-Nozzle-Expansion Ratio on Drag of Parabolic Afterbodies. NACA RM E54B12, 1954.

6. De Moraes, Carlos A., and Nowitzky, Albin M.: Experimental Effects of Propulsive Jets and Afterbody Configurations on the Zero-Lift Drag of Bodies of Revolution at a Mach Number of 1.59. NACA RM L54C16, 1954.

7. Cortright, Edgar M., and Schroeder, Albert H.: Preliminary Investigation of Effectiveness of Base Bleed in Reducing Drag of Blunt-Base Bodies in Supersonic Stream. NACA RM E51A26, 1951.

8. Love, Eugene S.: The Base Pressure at Supersonic Speeds on Two-Dimensional Airfoils and Bodies of Revolution (With and Without Fins) Having Turbulent Boundary Layers. NACA RM L53C02, 1953.

9. Coletti, Donald E.: Measurements and Predictions of Flow Conditions on a Two-Dimensional Base Separating a Mach Number 3.36 Jet and a Mach Number 1.55 Outer Stream. NACA RM L54C08, 1954.

10. Fraser, R. P., Connor, J. M., and Coulter, M. O.: The Measurement of the Reaction of Convergent, Convergent-Divergent and Inverted Nozzles at High Pressure. Ministry of Supply Rep., Imperial College of Science (London), M.O.S. EMR F72/204, May 1946.

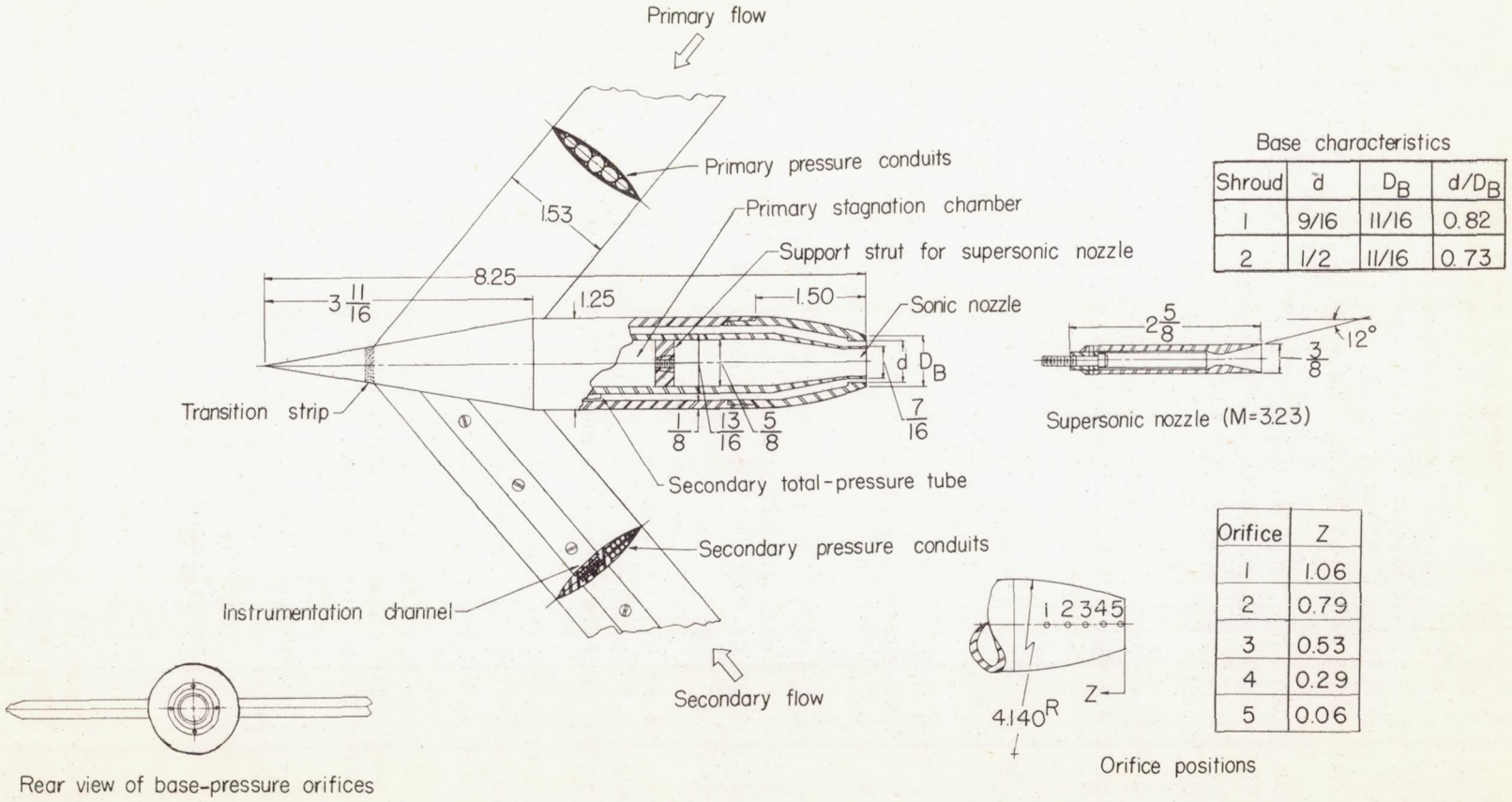

Base characteristics

Shroud	d	D_B	d/D_B
1	9/16	11/16	0.82
2	1/2	11/16	0.73

Orifice	Z
1	1.06
2	0.79
3	0.53
4	0.29
5	0.06

Figure 1.- Sketch of model and wing supports. All dimensions are in inches.

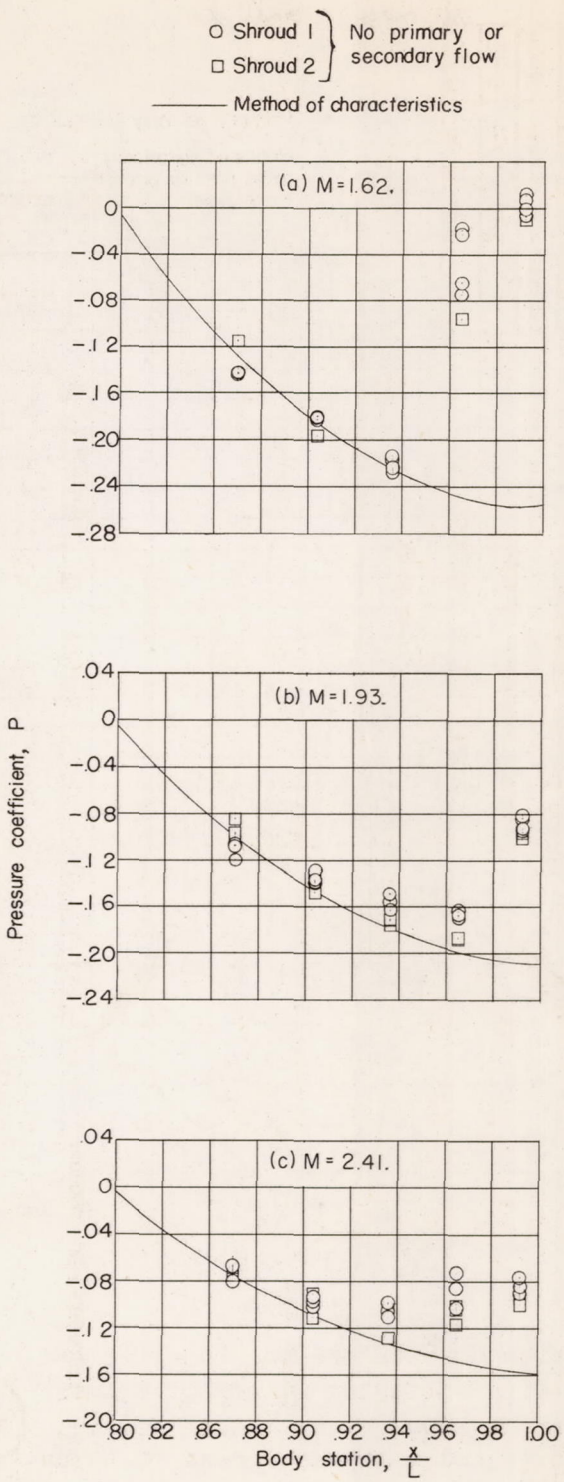

Figure 2.- Comparison of experimental boattail pressure distributions of both shrouds with method of characteristics for free-stream Mach numbers of 1.62, 1.93, and 2.41.

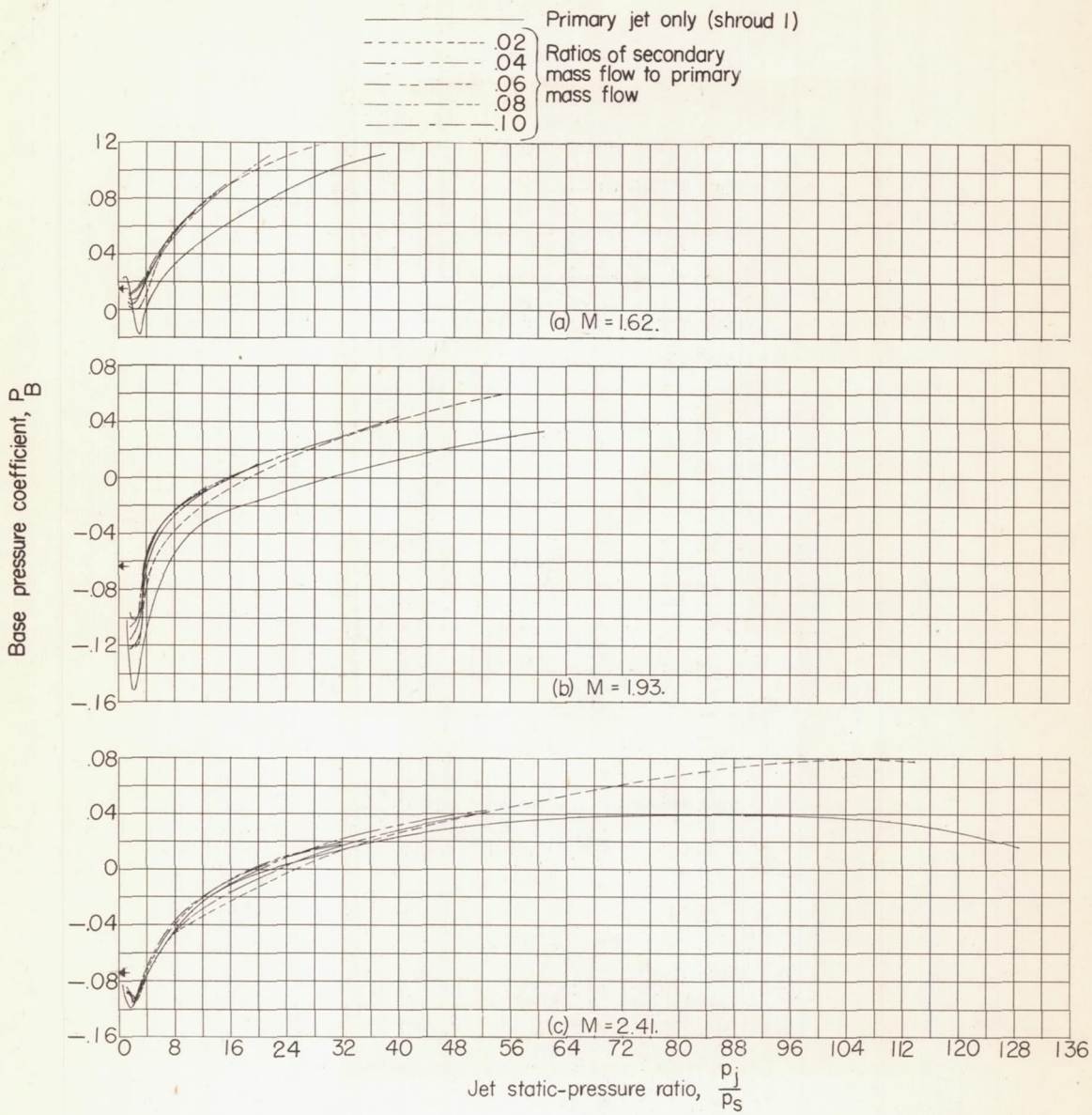

Figure 3.- Variation of base pressure coefficient of first shroud (d/D_B = 0.82) with different values of primary jet pressure ratio and secondary mass-flow ratio. Sonic nozzle; M = 1.62, 1.93, and 2.41. Arrows indicate base-pressure values for no primary or secondary flow.

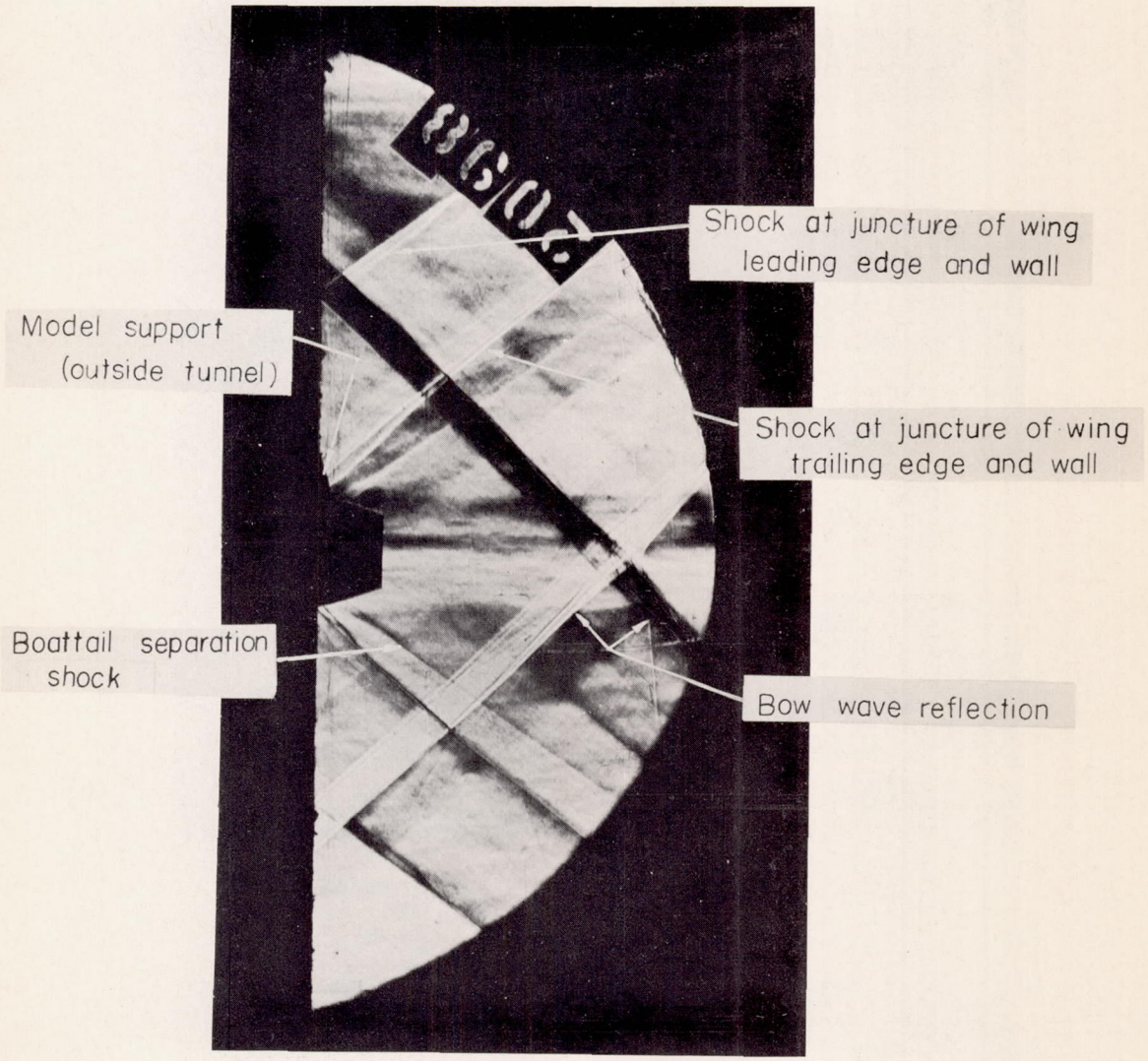

L-85662

Figure 4.- Typical full-size schlieren photograph illustrating the tunnel flow at a free-stream Mach number of 1.62.

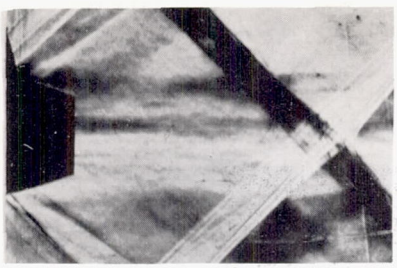

No flow

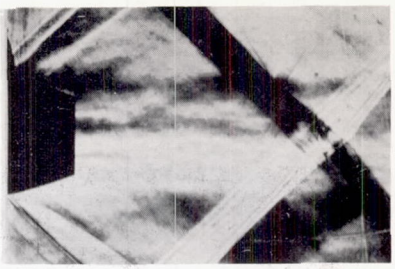

$p_j/p_s = 1.17$

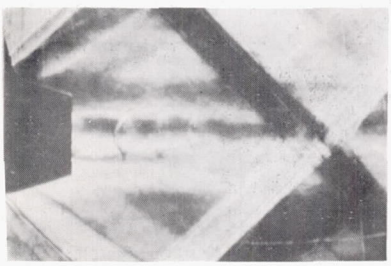

$p_j/p_s = 1.93$

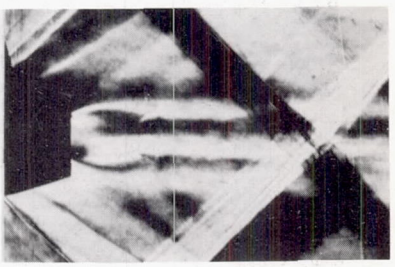

$p_j/p_s = 4.18$

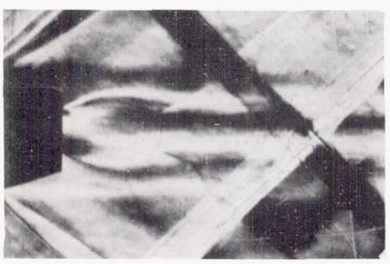

$p_j/p_s = 6.95$

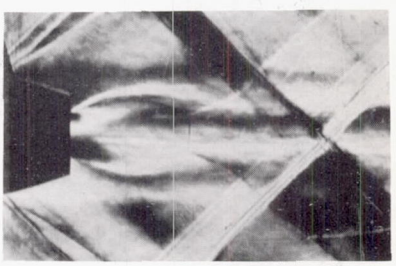

$p_j/p_s = 9.26$

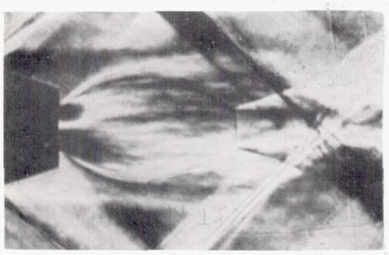

$p_j/p_s = 17.65$

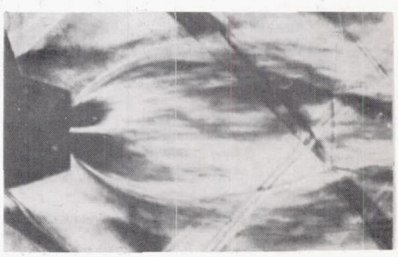

$p_j/p_s = 38.14$

L-85663

Figure 5.- Schlieren photographs for first shroud ($d/D_B = 0.82$) at various jet pressure ratios. Sonic nozzle; M = 1.62.

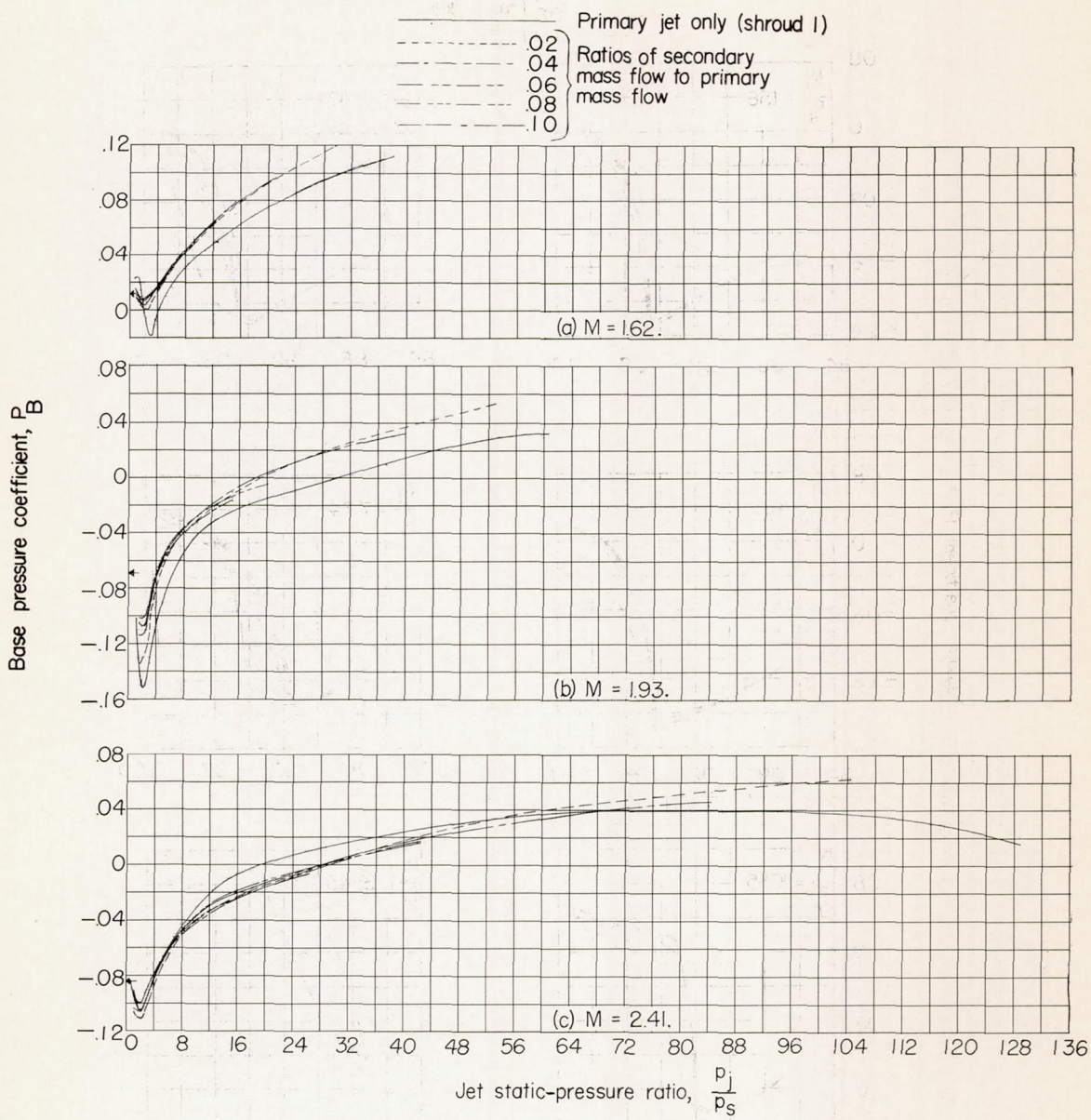

Figure 6.- Variation of base pressure coefficient of second shroud (d/D_B = 0.73) with different values of primary jet pressure ratio and secondary mass-flow ratio. Sonic nozzle; M = 1.62, 1.93, and 2.41. Arrows indicate base-pressure values for no primary or secondary flow.

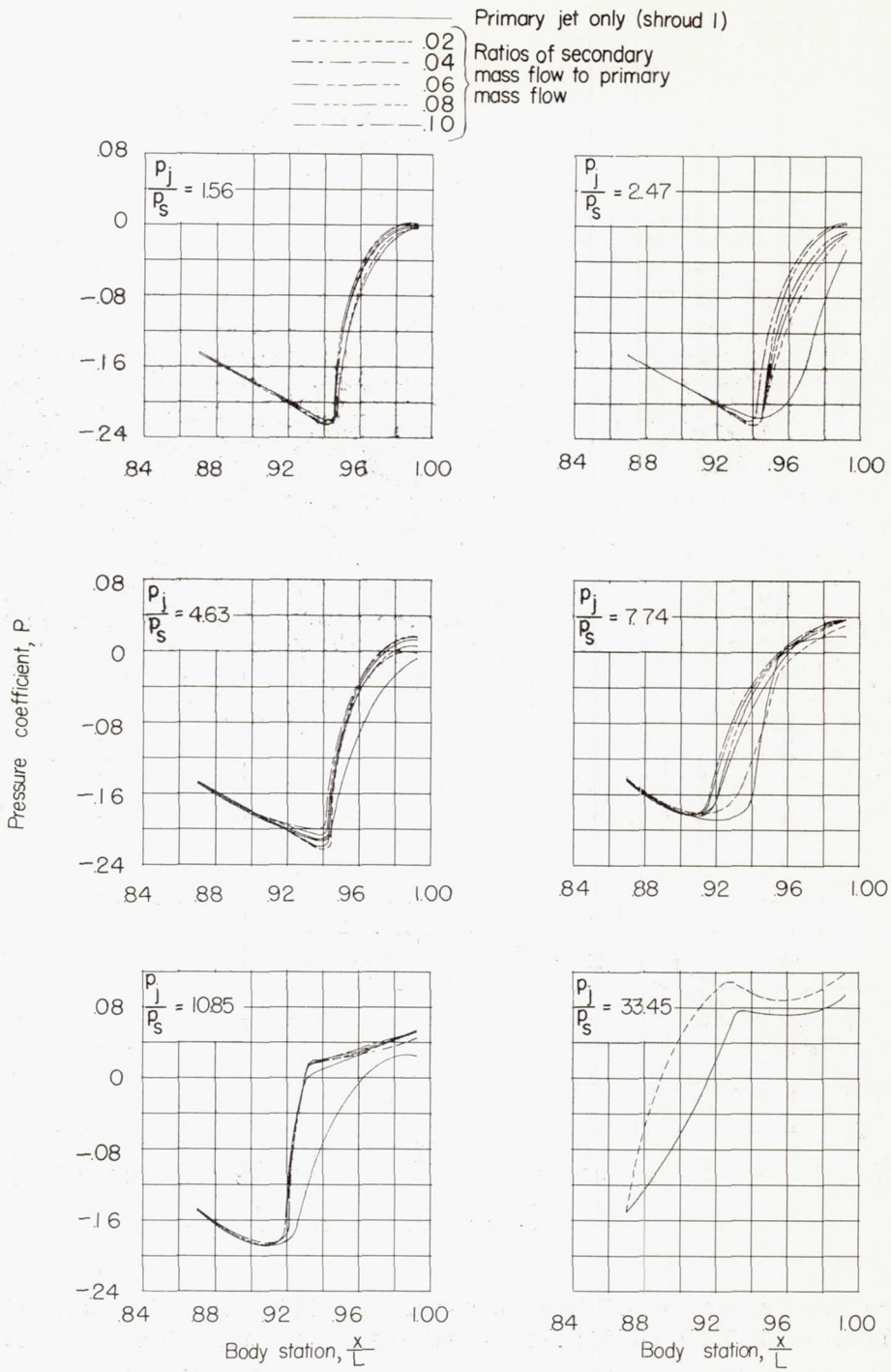

(a) M = 1.62.

Figure 7.- Variation of boattail pressure coefficient on first shroud (d/D_B = 0.82) for different values of primary jet pressure ratio and secondary mass-flow ratio. Sonic nozzle.

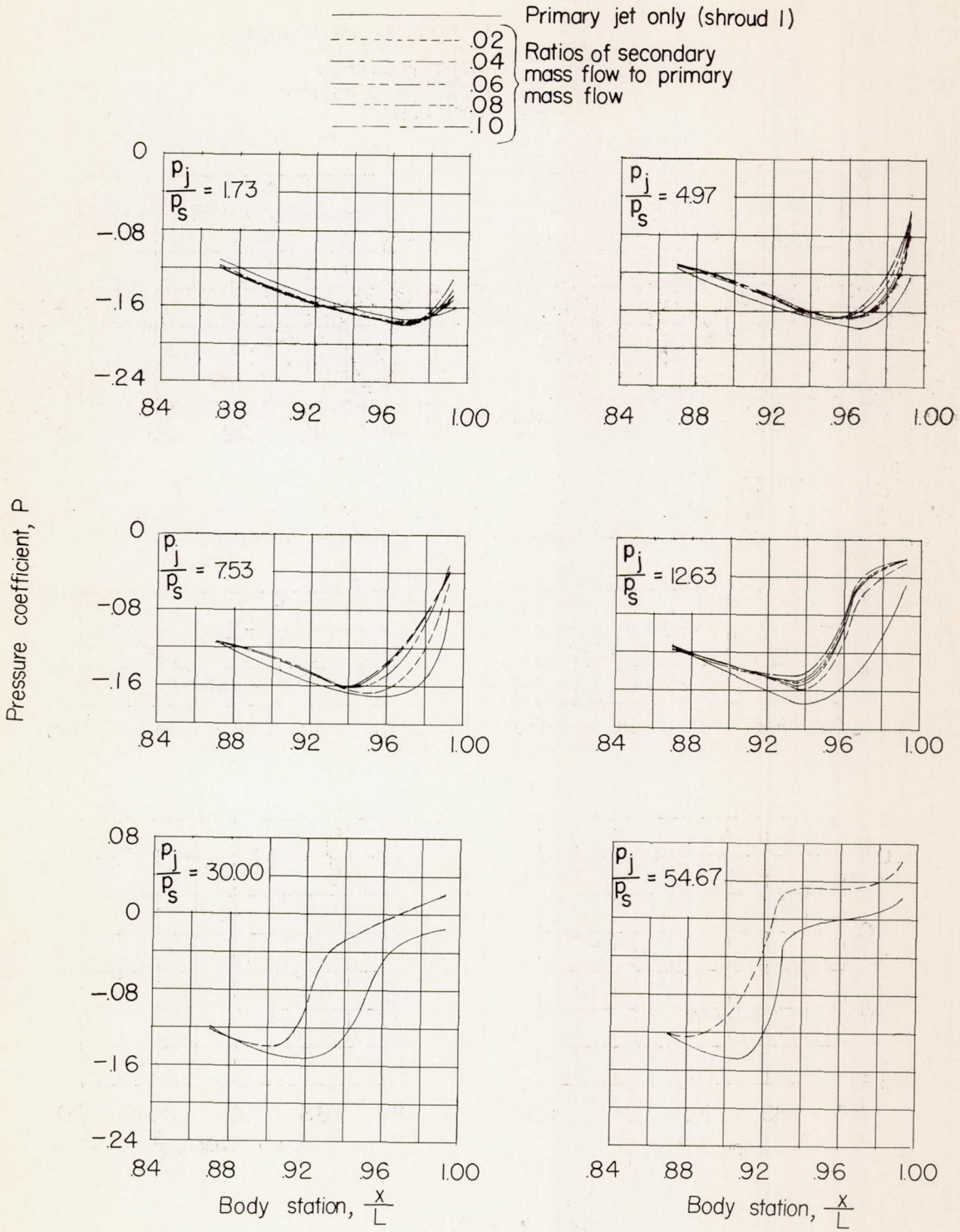

(b) M = 1.93.

Figure 7.- Continued.

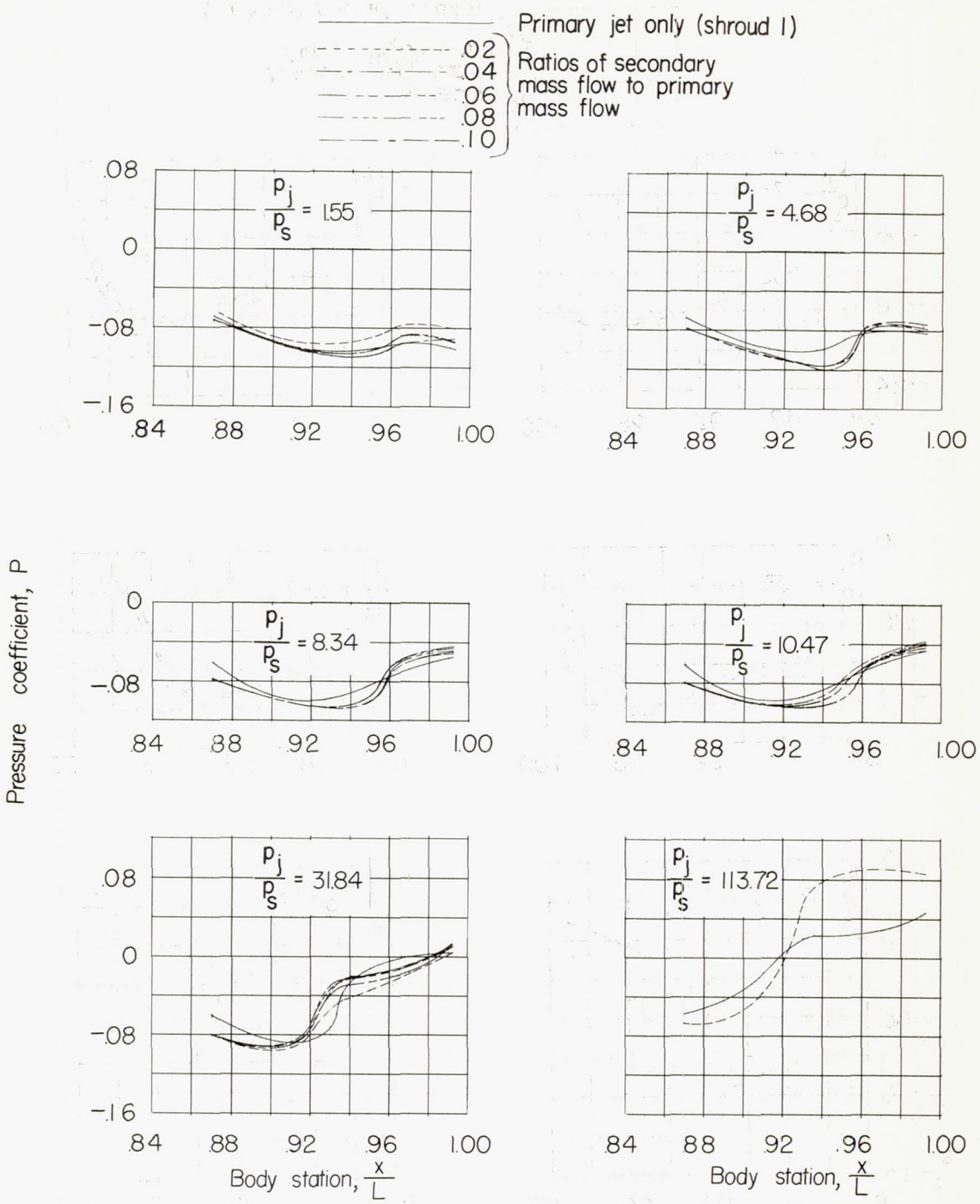

(c) M = 2.41.

Figure 7.- Concluded.

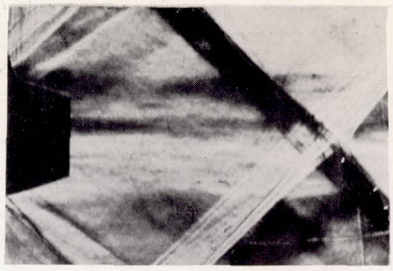

No flow

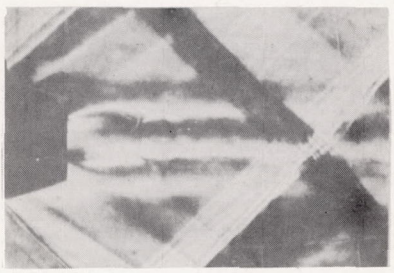

$p_j/p_s = 4.65$; w=0

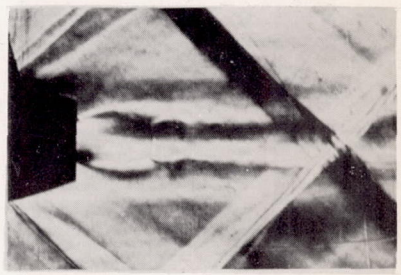

$p_j/p_s = 4.65$; w=.02

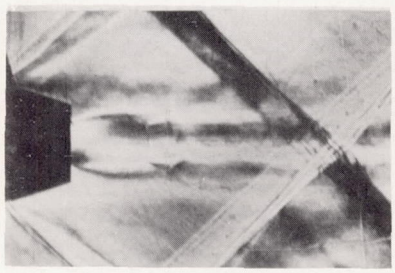

$p_j/p_s = 4.65$; w=.04

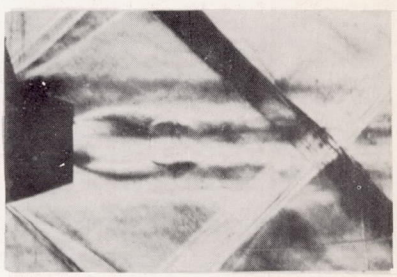

$p_j/p_s = 4.65$; w=.06

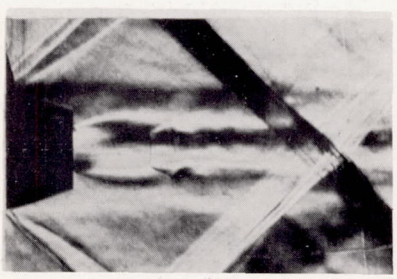

$p_j/p_s = 4.65$; w=.08

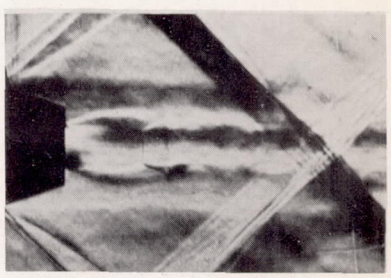

$p_j/p_s = 4.65$; w=.10

L-85664

Figure 8.- Schlieren photographs for first shroud at M = 1.62 illustrating flow mechanism of sonic nozzle at jet static-pressure ratio of 4.65 and various secondary mass-flow ratios.

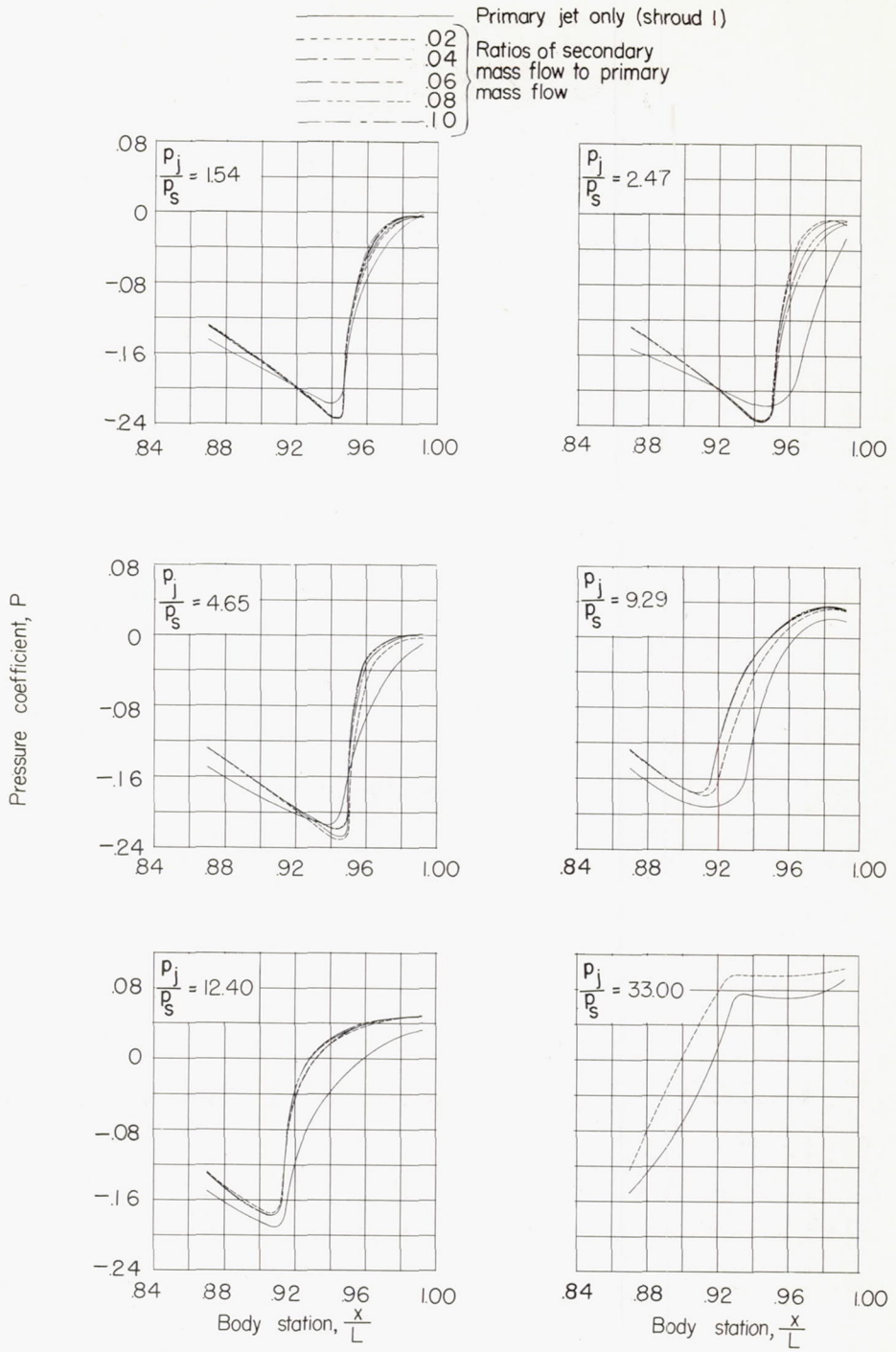

(a) M = 1.62.

Figure 9.- Variation of boattail pressure coefficient on second shroud (d/D_B = 0.73) for different values of primary jet pressure ratio and secondary mass-flow ratio. Sonic nozzle.

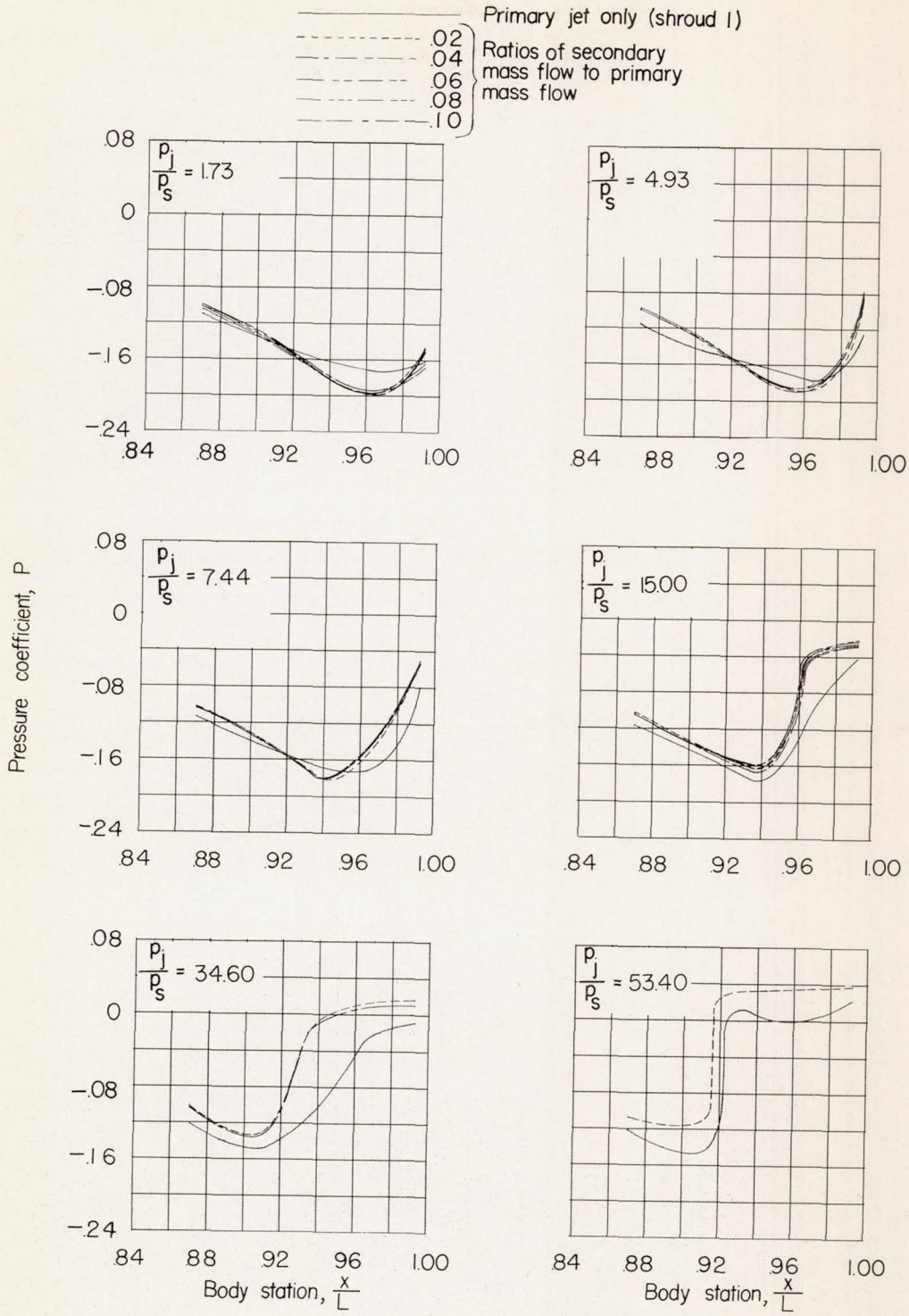

(b) M = 1.93.

Figure 9.- Continued.

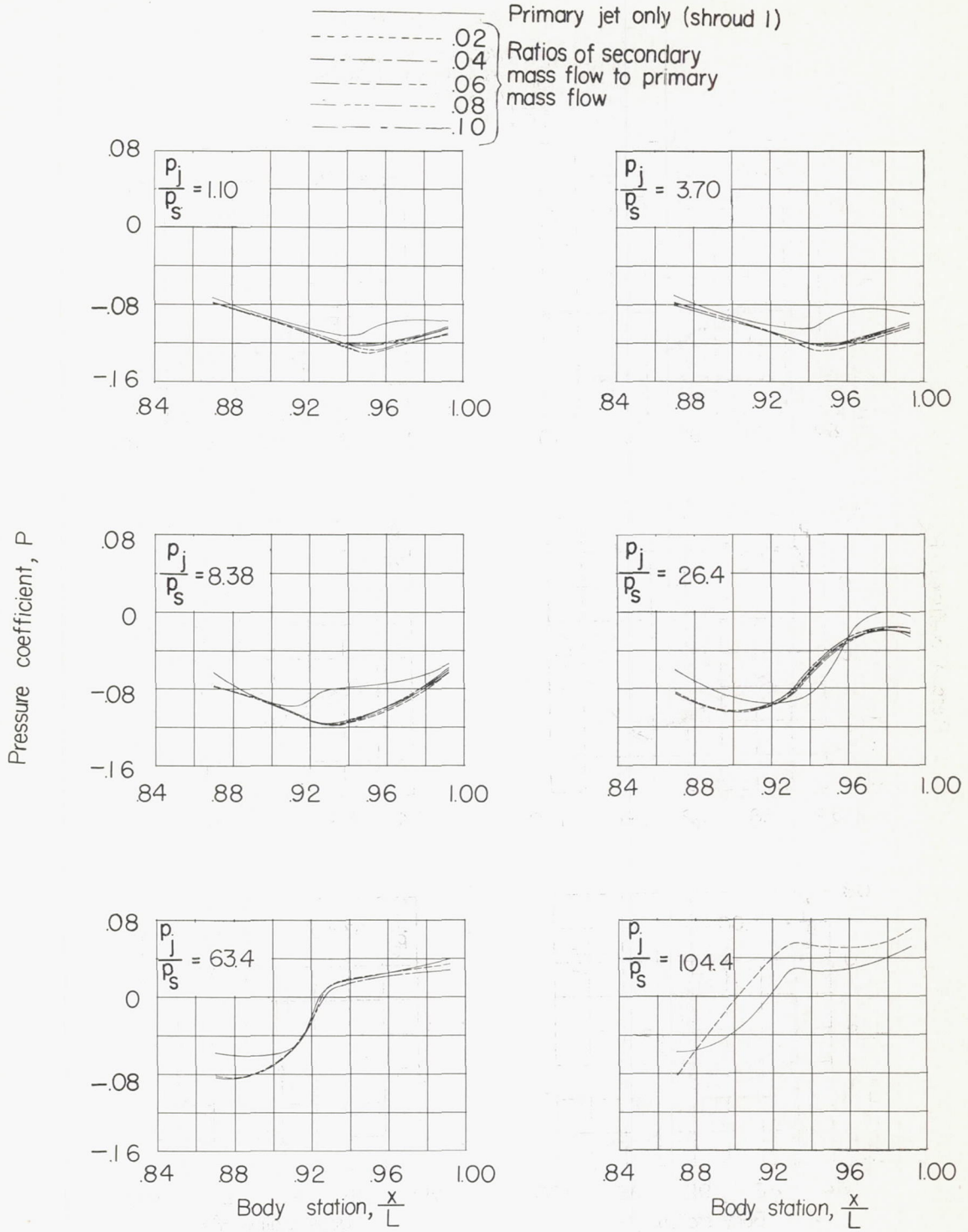

(c) M = 2.41.

Figure 9.- Concluded.

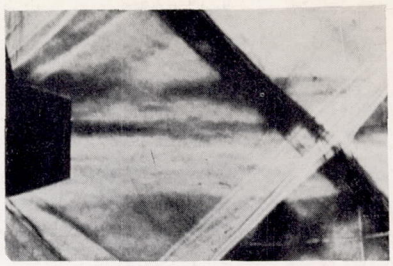

No flow

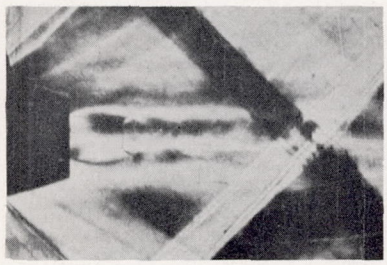

p_j/p_s = 3.10; w = 0

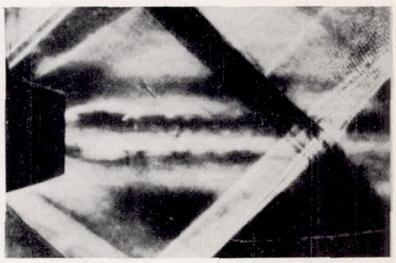

p_j/p_s = 3.10; w = .02

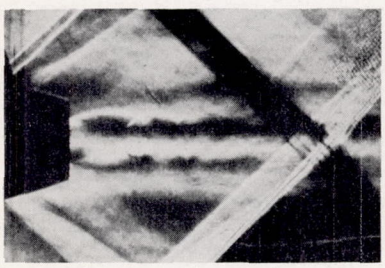

p_j/p_s = 3.10; w = .04

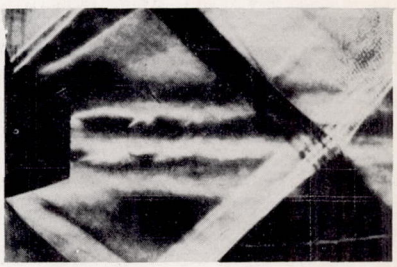

p_j/p_s = 3.10; w = .06

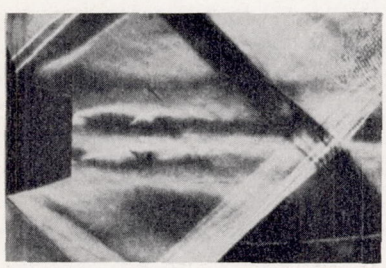

p_j/p_s = 3.10; w = .08

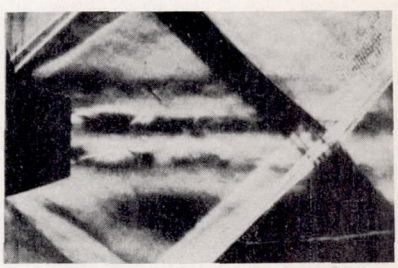

p_j/p_s = 3.10; w = .10

L-85665

Figure 10.- Schlieren photographs for second shroud at M = 1.62 illustrating flow mechanism of sonic nozzle at jet static-pressure ratio of 3.10 together with various secondary mass-flow ratios.

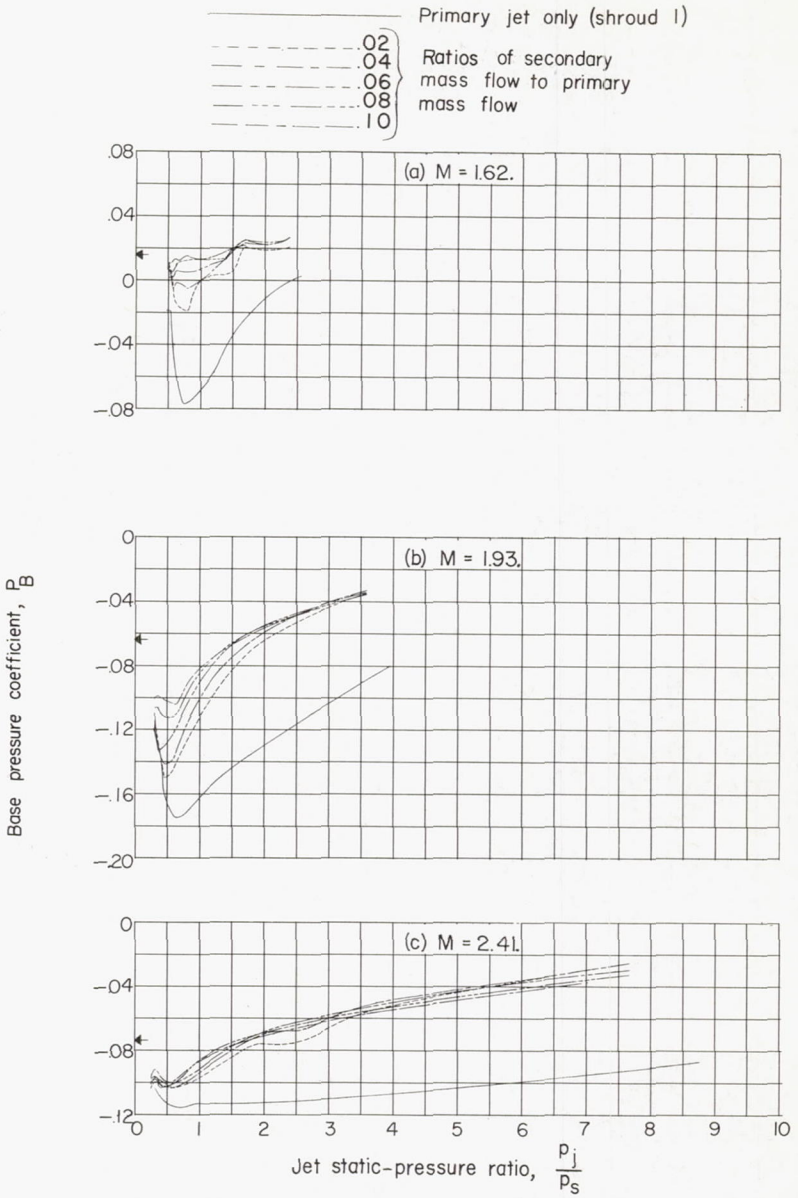

Figure 11.- Variation of base pressure coefficient of first shroud (d/D_B = 0.82) with different values of primary jet pressure ratio and secondary mass-flow ratio. Supersonic nozzle; M = 1.62, 1.93, and 2.41. Arrows indicate base-pressure values for no primary or secondary flow.

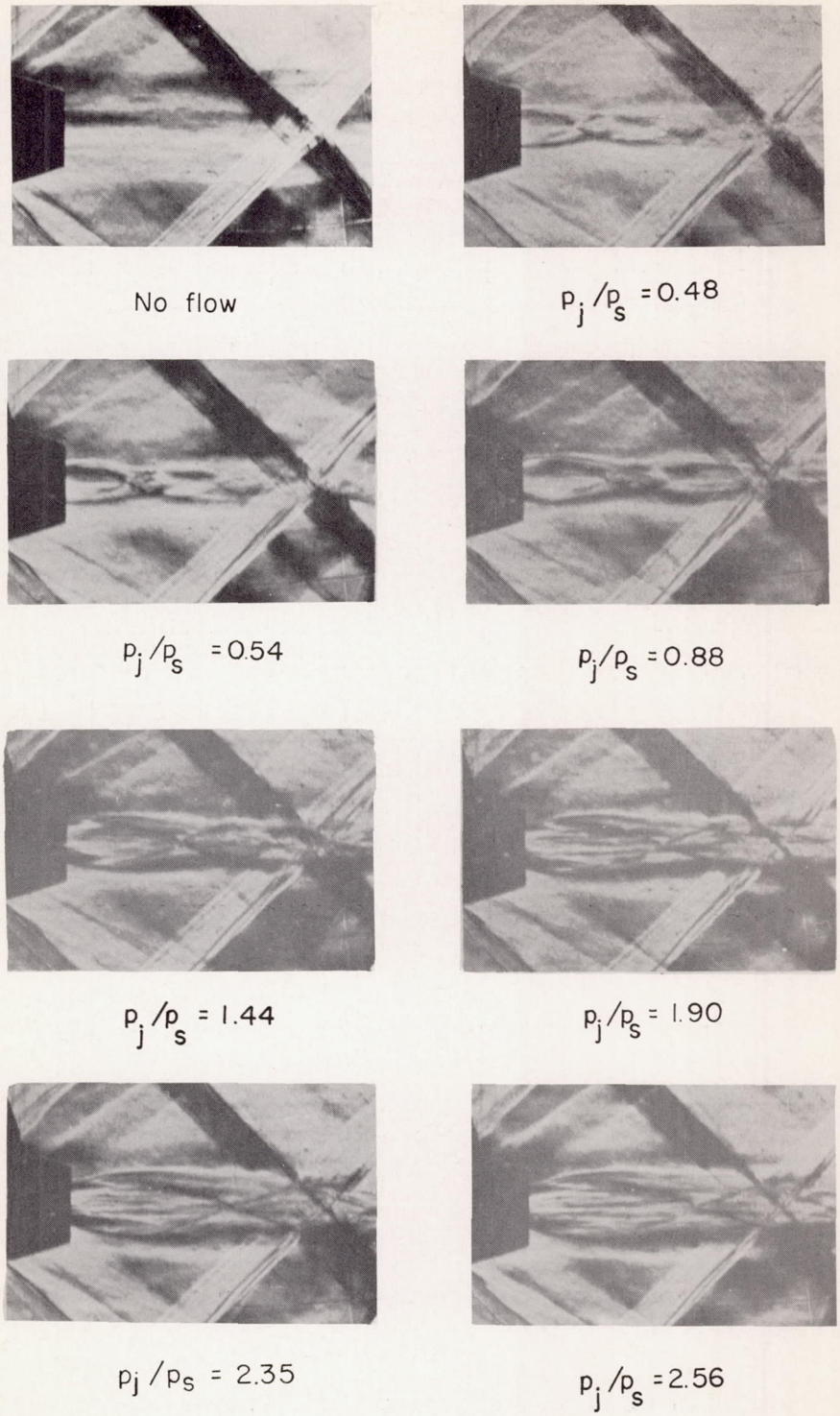

L-85666

Figure 12.- Schlieren photographs for first shroud (d/D_B = 0.82) at various jet pressure ratios. Supersonic nozzle; M = 1.62.

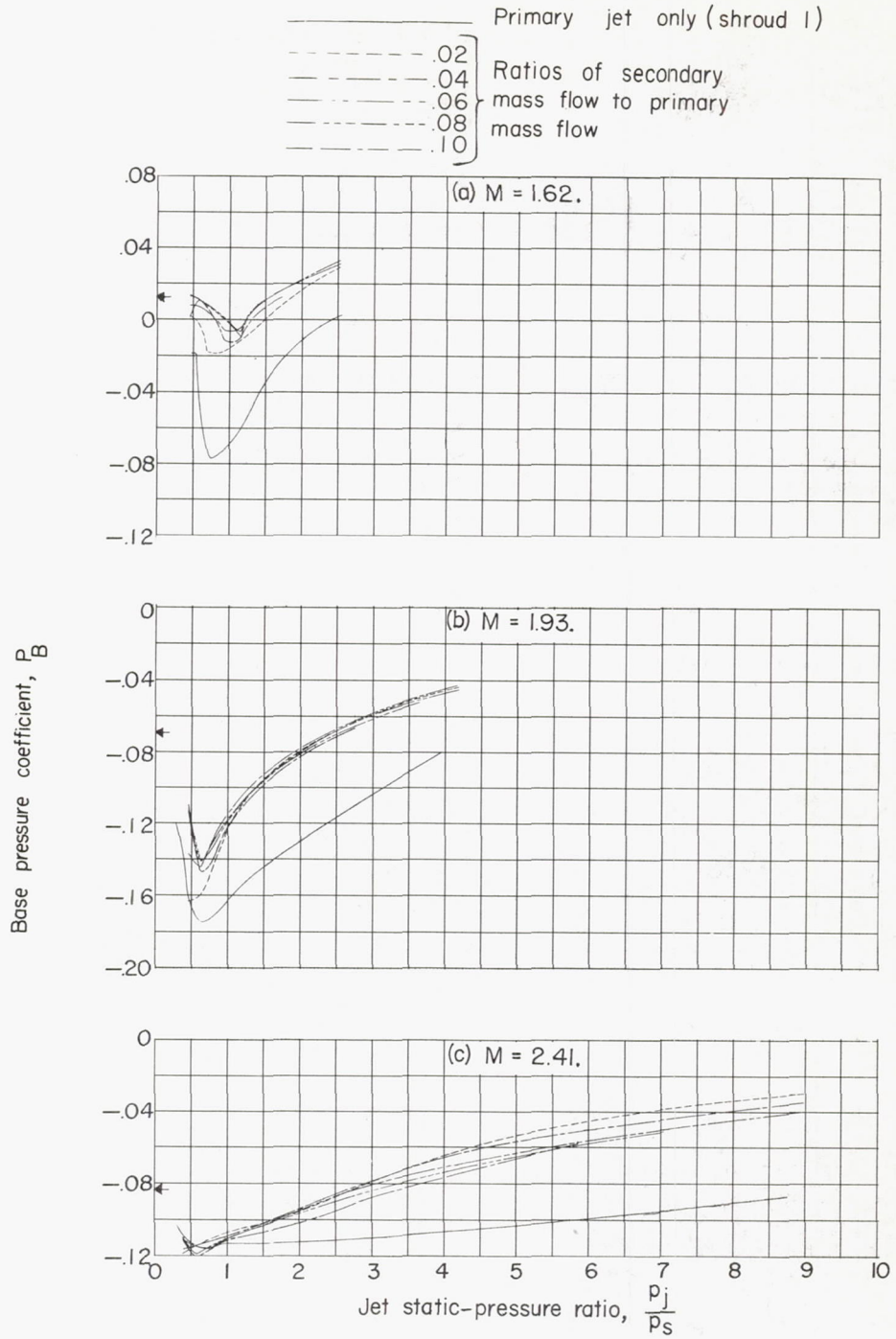

Figure 13.- Variation of base pressure coefficient of second shroud (d/D_B = 0.73) with different values of primary jet pressure ratio and secondary mass-flow ratio. Supersonic nozzle; M = 1.62, 1.93, and 2.41. Arrows indicate base-pressure values for no primary or secondary flow.

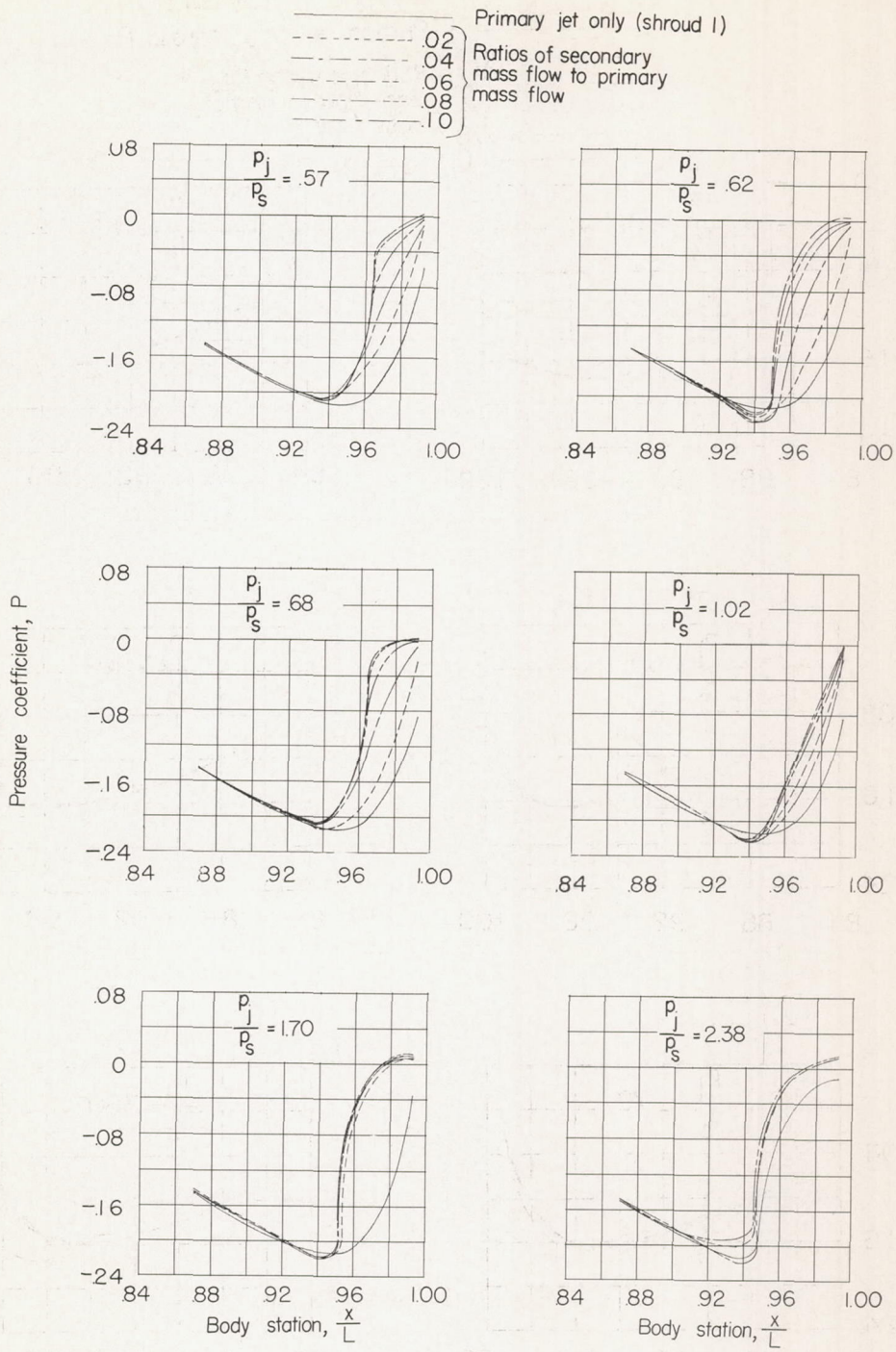

(a) M = 1.62.

Figure 14.- Variation of boattail pressure coefficient on first shroud (d/D_B = 0.82) for different values of primary jet pressure ratio and secondary mass-flow ratio. Supersonic nozzle.

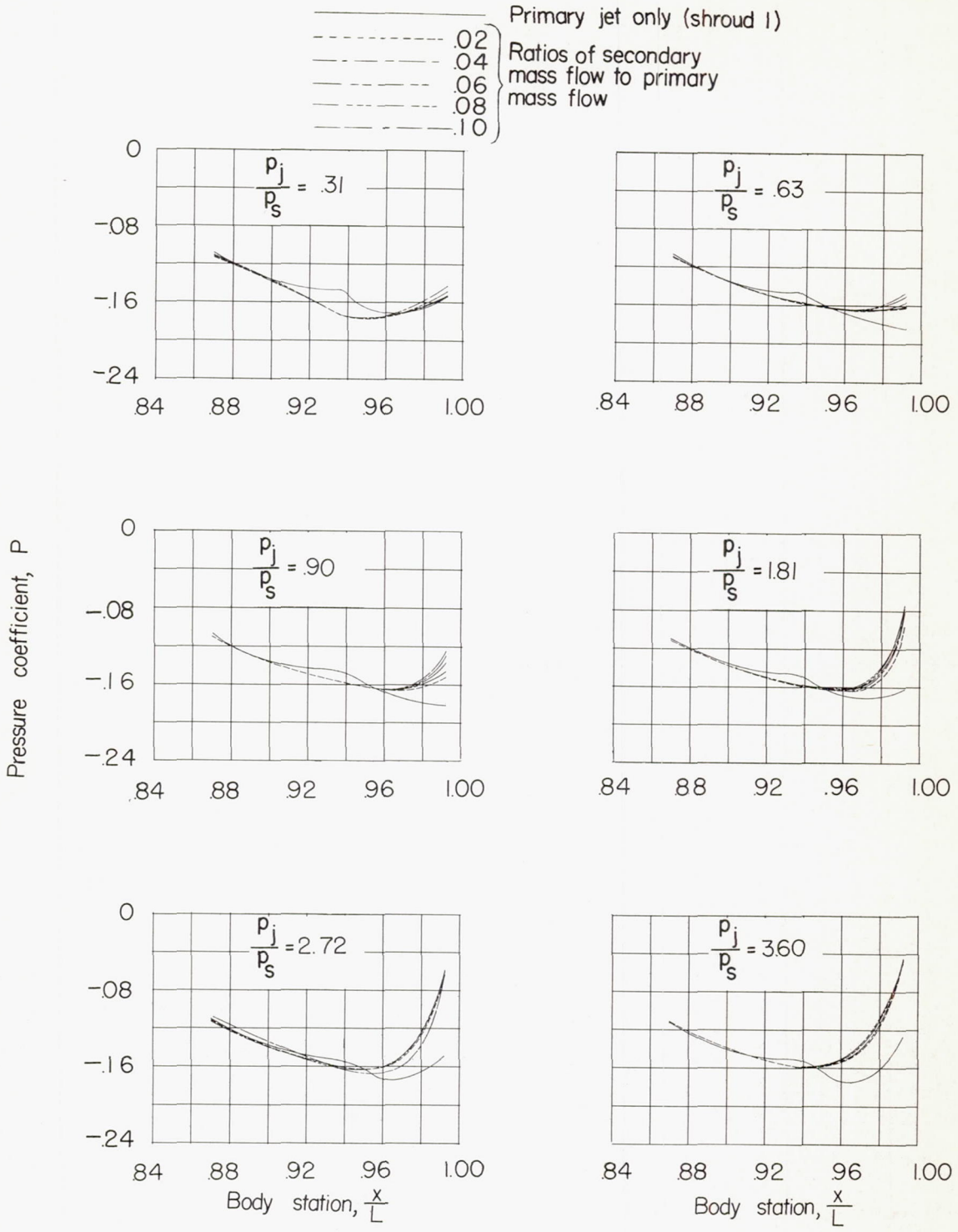

(b) M = 1.93.

Figure 14.- Continued.

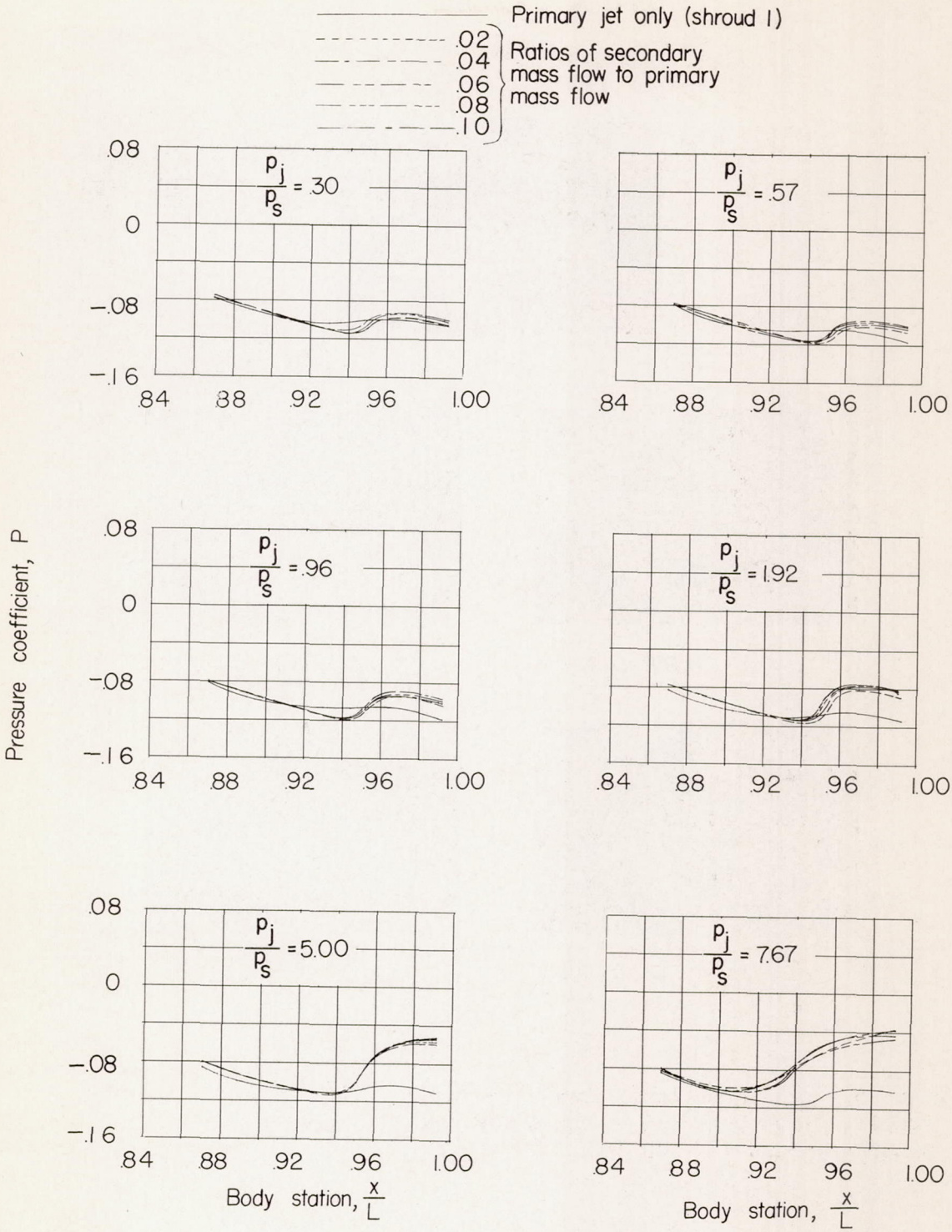

(c) M = 2.41.

Figure 14.- Concluded.

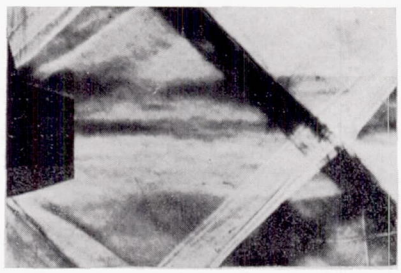

No flow

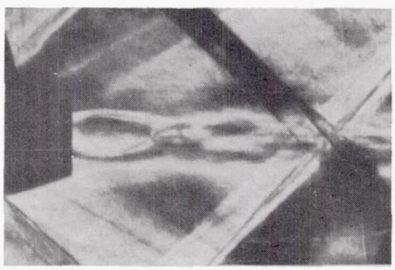

$p_j/p_s = 0.76; w = 0$

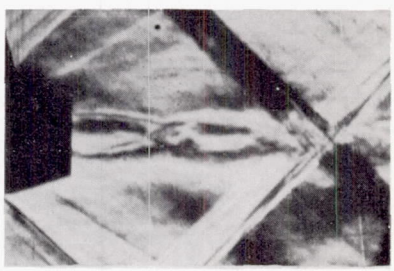

$p_j/p_s = 0.68; w = .02$

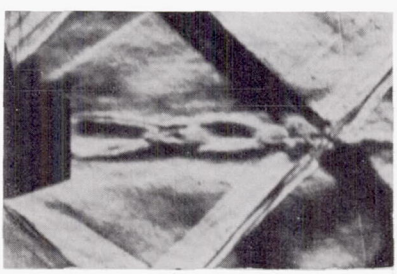

$p_j/p_s = 0.68; w = .04$

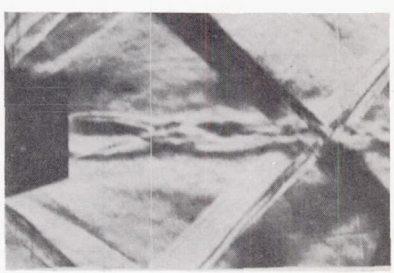

$p_j/p_s = 0.68; w = .06$

L-85667

Figure 15.- Schlieren photographs for first shroud at M = 1.62 illustrating flow mechanism of supersonic nozzle together with various secondary mass-flow ratios.

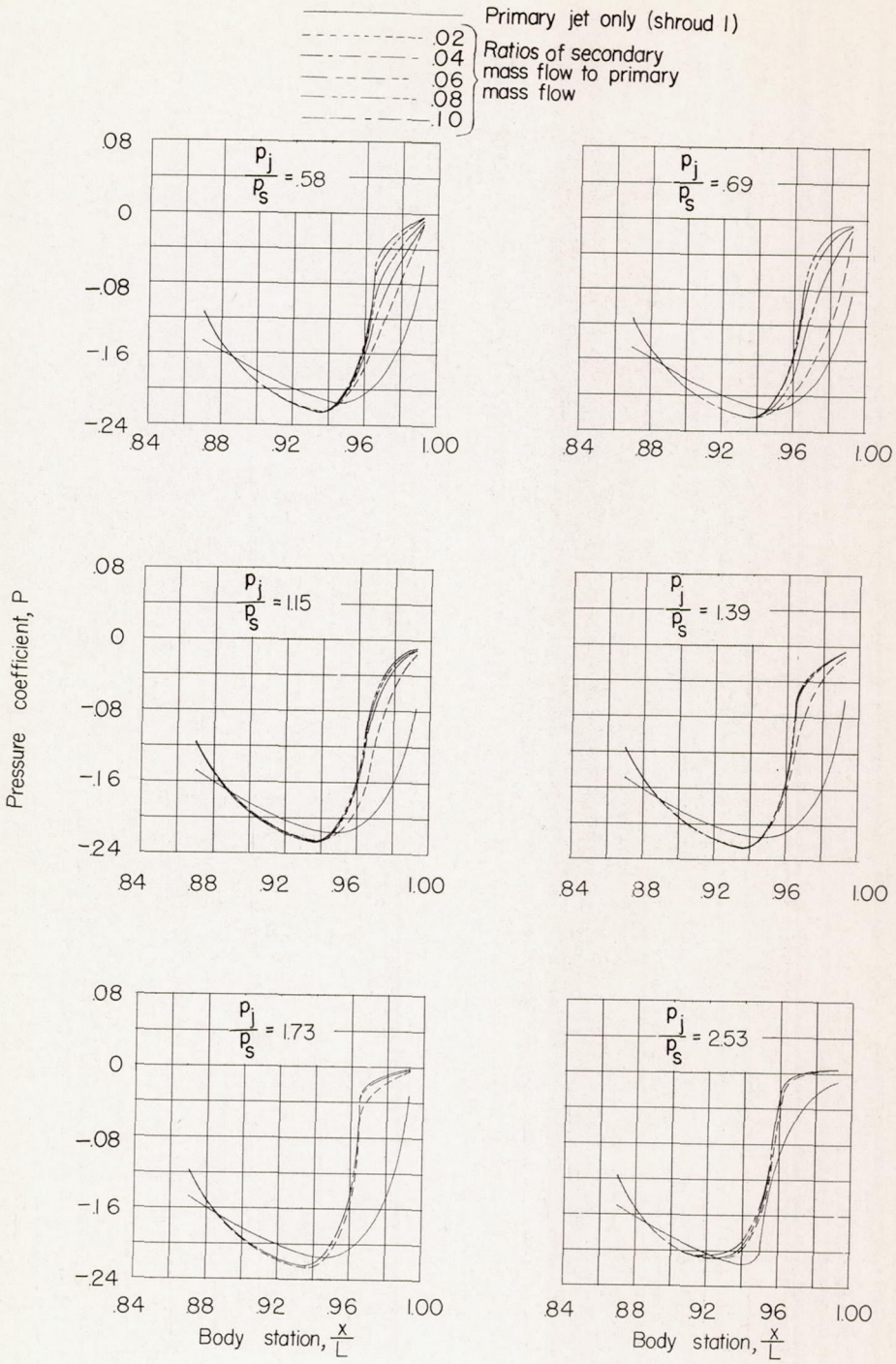

(a) M = 1.62.

Figure 16.- Variation of boattail pressure coefficient on second shroud (d/D_B = 0.73) for different values of primary jet pressure ratio and secondary mass-flow ratio. Supersonic nozzle.

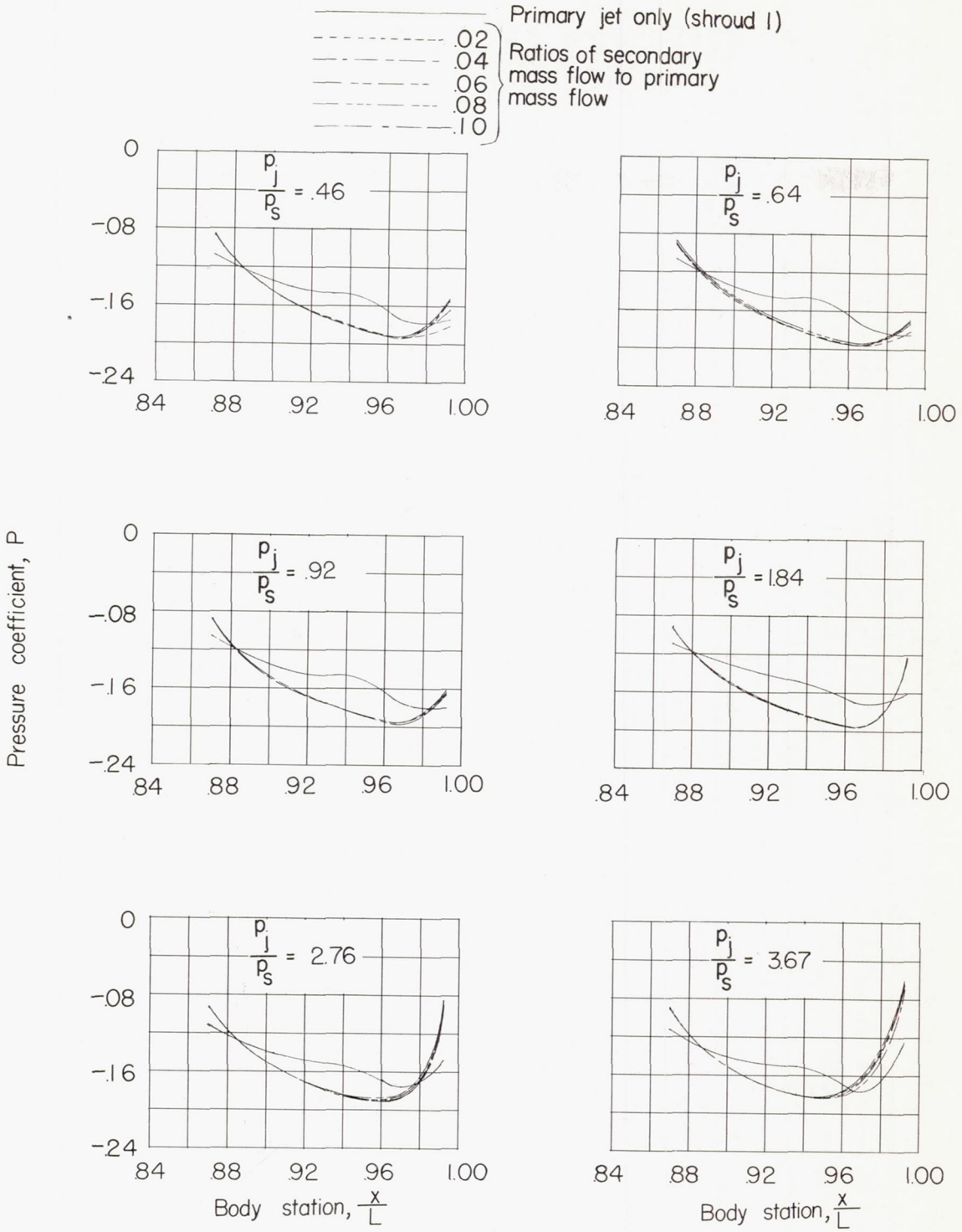

(b) M = 1.93.

Figure 16.- Continued.

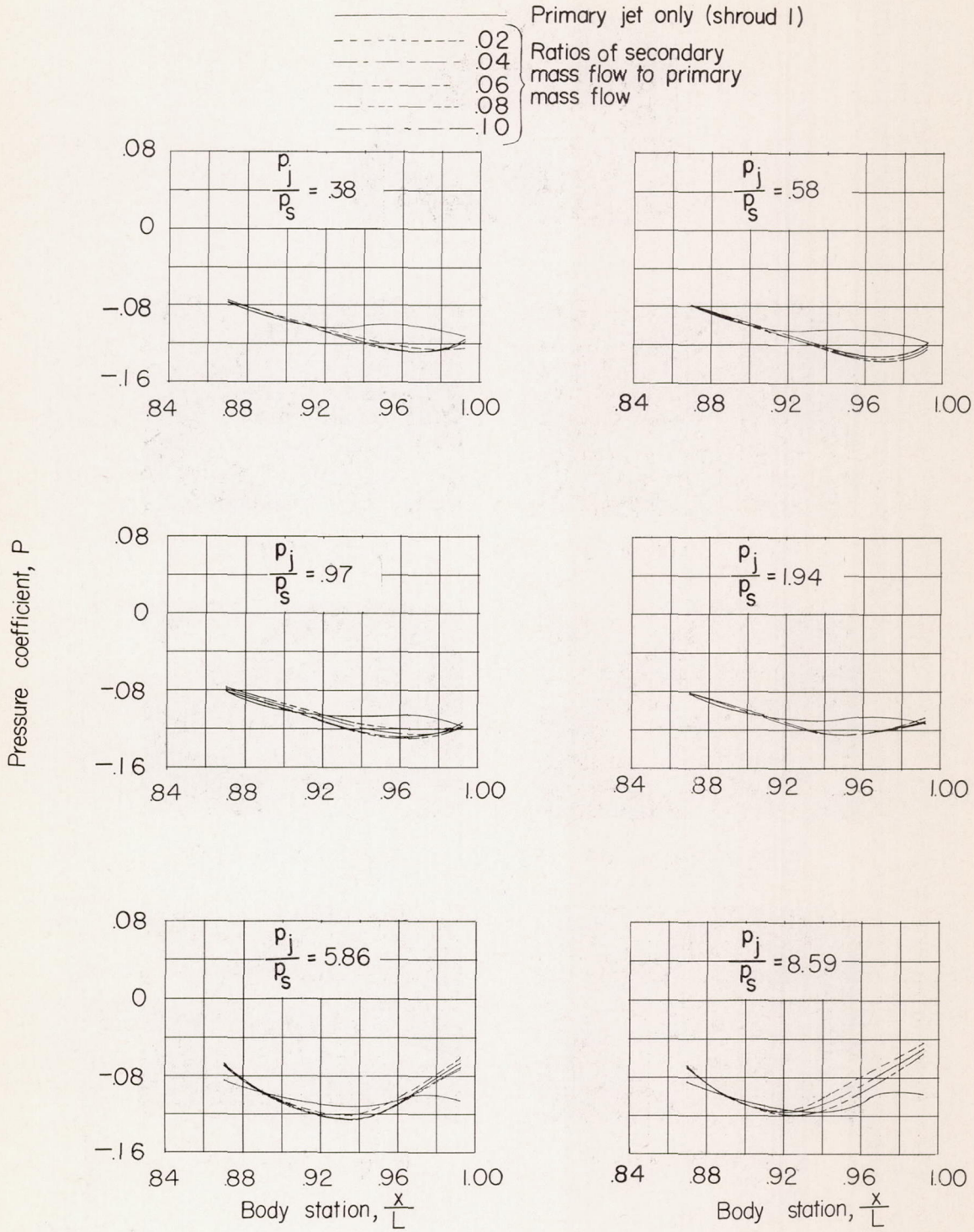

(c) M = 2.41.

Figure 16.- Concluded.

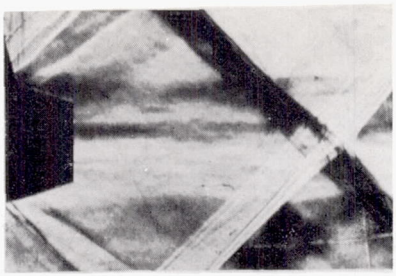

No flow

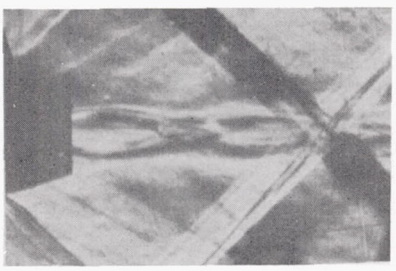

$p_j/p_s = 0.88$; $w = 0$

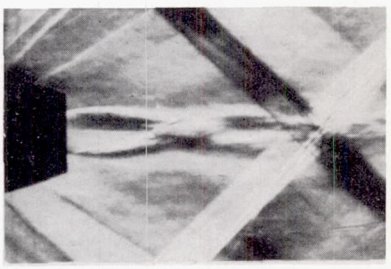

$p_j/p_s = 0.92$; $w = .02$

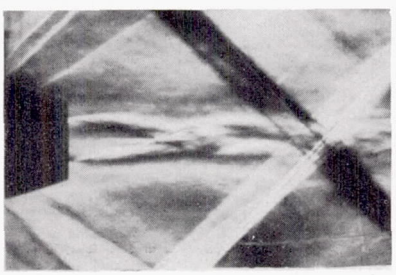

$p_j/p_s = 0.92$; $w = .04$

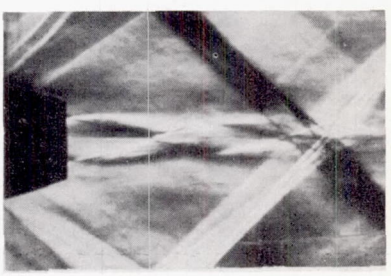

$p_j/p_s = 0.92$; $w = .06$

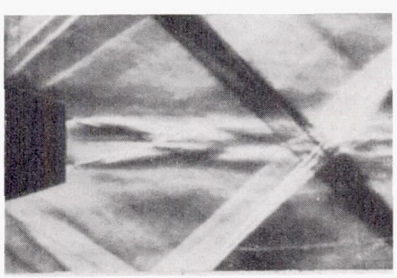

$p_j/p_s = 0.92$; $w = .08$

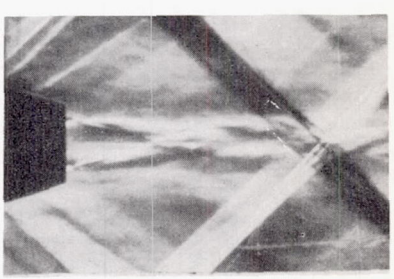

$p_j/p_s = 0.92$; $w = .10$

L-85668

Figure 17.- Schlieren photographs for second shroud at $M = 1.62$ illustrating flow mechanism of supersonic nozzle together with various secondary mass-flow ratios.

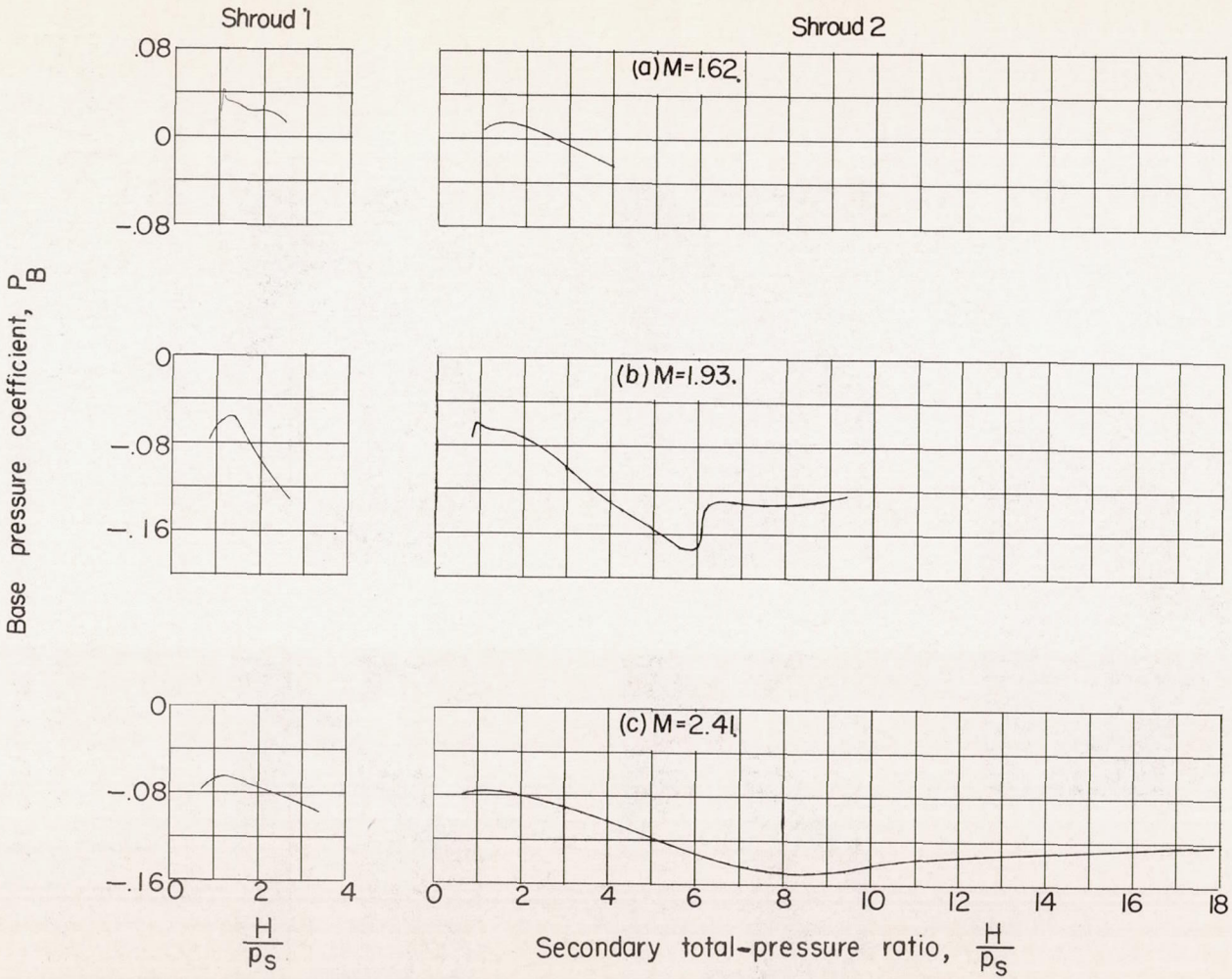

Figure 18.- Variation of base pressure coefficient of both shrouds with different values of secondary total-pressure ratio at free-stream Mach numbers of 1.62, 1.93, and 2.41.

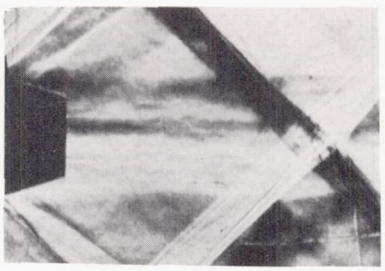

No flow

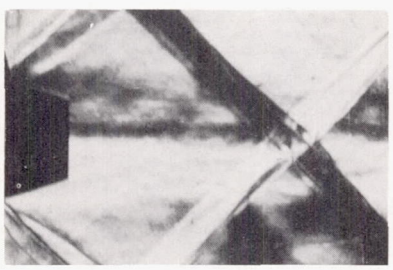

H/p_s = 1.04

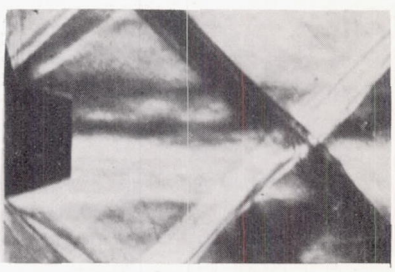

H/p_s = 1.07

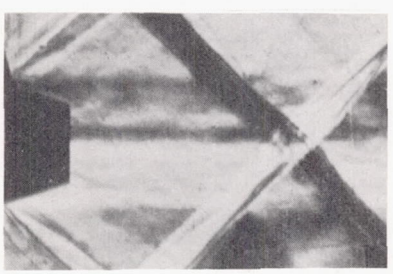

H/p_s = 1.61

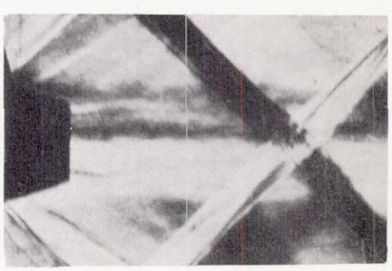

H/p_s = 2.50

L-85669

Figure 19.- Schlieren photographs at M = 1.62 for first shroud at various secondary total-pressure ratios.

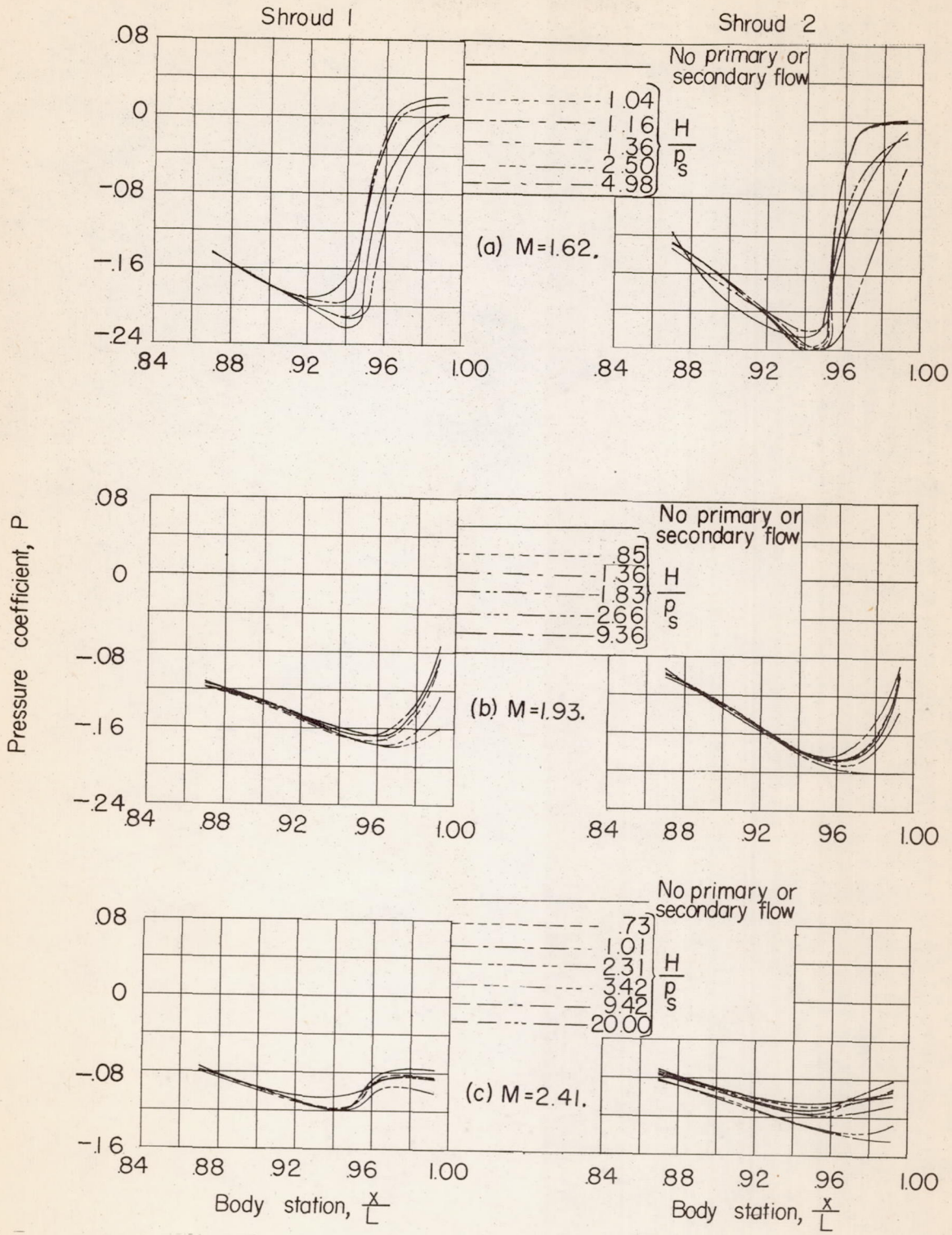

Figure 20.- Effects of secondary mass flow on pressure distributions of both shrouds at M = 1.62, 1.93, and 2.41.